AD-A133 772 E-BEAM WRITTEN COMPUTER GENERATED HOLOGRAMS(U) 1/1
HONEYWELL CORPORATE TECHNOLOGY CENTER BLOOMINGTON MN
S M ARNOLD AUG 83 E47069 AFOSR-TR-83-0850
UNCLASSIFIED F49620-80-C-0029 F/G 14/5 NL

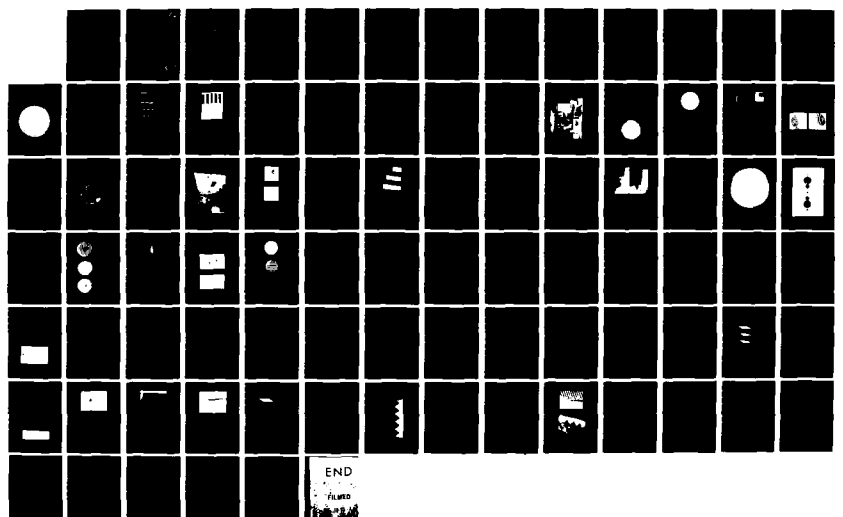

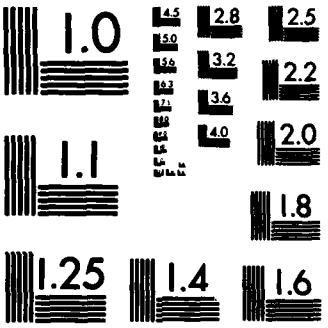

AFOSR-TR- 83-0850

13

E-BEAM WRITTEN COMPUTER GENERATED HOLOGRAMS

Final Technical Report
on F49620-80-C-0029
AFOSR Contract No. [redacted]

Steven M. Arnold
Honeywell Corporate Technology Center
Bloomington, Minnesota 55420
Tel. 612-887-4461

August 1983

Directorate of Electronics & Material Sciences
AFOSR/NE, Building 410
Bolling AFB
Washington, D.C. 20332

E-BEAM WRITTEN COMPUTER GENERATED HOLOGRAMS

Final Technical Report
on F49620-80-C-0029
AFOSR Contract No: [redacted]

Steven M. Arnold
Honeywell Corporate Technology Center
Bloomington, Minnesota 55420

August 1983

Approved By: L D Hutcheson
Lynn Hutcheson, Electro-Optics Group Leader

Obert Tufte
Obert Tufte, Department Manager

UNCLASSIFIED
SECURITY CLASSIFICATION OF THIS PAGE (WHEN DATA ENTERED)

REPORT DOCUMENTATION PAGE		READ INSTRUCTIONS BEFORE COMPLETING FORM
1. REPORT NUMBER AFOSR-TR- 83-0850	2. GOV'T ACCESSION NUMBER AD-A133 772	3. RECIPIENT'S CATALOG NUMBER
4. TITLE (AND SUBTITLE) E-beam Written Computer Generated Holograms		5. TYPE OF REPORT/PERIOD COVERED Final Technical Report 1 January 1980 – 28 February 1983
		6. PERFORMING ORG. REPORT NUMBER E47069
7. AUTHOR(S) Steven M. Arnold		8. CONTRACT OR GRANT NUMBER(S) [redacted] F49620-80-C-0029
9. PERFORMING ORGANIZATIONS NAME/ADDRESS Honeywell Corporate Technology Center 10701 Lyndale Avenue South Bloomington, Minnesota 55420		10. PROGRAM ELEMENT, PROJECT, TASK AREA & WORK UNIT NUMBERS 61102F 2305/B2
11. CONTROLLING OFFICE NAME/ADDRESS		12. REPORT DATE August 1983
		13. NUMBER OF PAGES 80
14. MONITORING AGENCY NAME/ADDRESS (IF DIFFERENT FROM CONT. OFF.) Office of Electronic and Solid State Sciences AFOSR, Bldg 410 Bolling AFB, Washington, D.C. 20332		15. SECURITY CLASSIFICATION (OF THIS REPORT) Unclassified
		15a. DECLASSIFICATION DOWNGRADING SCHEDULE

16. DISTRIBUTION STATEMENT (OF THIS REPORT)
Approved for public release: distribution unlimited

17. DISTRIBUTION STATEMENT (OF THE ABSTRACT ENTERED IN BLOCK 20, IF DIFFERENT FROM REPORT)

18. SUPPLEMENTARY NOTES
Dr. John A. Neff was the contract monitor for this program.

19. KEY WORDS (CONTINUE ON REVERSE SIDE IF NECESSARY AND IDENTIFY BY BLOCK NUMBER)

Computer Generated Hologram	Optical Testing
E-beam Lithography	Optical Computing
Holographic Optical Element	Diffraction

20. ABSTRACT (CONTINUE ON REVERSE SIDE IF NECESSARY AND IDENTIFY BY BLOCK NUMBER)
This final report describes a three-year research program to investigate computer generated holograms produced by electron beam lithography. Because they are light weight and can create wavefronts of arbitrary complexity, computer generated holograms are attractive for applications such as optical data processing and optical testing. To be practical, these elements must have large space-bandwidth products, and have the qualities of high diffraction efficiency, low scattering, low aberration and low cost, as compared to conventional optics. We have developed generalized encoding algorithms and fabrication techniques for producing e-beam computer generated holograms having submicron feature sizes, distortion-free resolution of better than 0.4 micron, and space-bandwidth products in excess of 10^7. E-beam lithography is superior to optical plotting for writing computer generated holograms and,

HD-168 REV 11/74

DD FORM 1 JAN 73 1473 EDITION OF 1 NOV 55 IS OBSOLETE

UNCLASSIFIED
SECURITY CLASSIFICATION OF THIS PAGE (WHEN DATA ENTERED)

with further refinement, could be extended to produce holograms having space-bandwidth products as large as 10^{11}, comparing favorably with interferometrically recorded holograms.

We have demonstrated the application of e-beam computer generated holograms to the testing of asymmetric, aspheric optics having up to 123 waves of aspheric aberration. We have also developed an optical vector-matrix multiplication scheme that utilizes e-beam computer generated holograms to achieve high numerical accuracy and large numerical range; an accuracy of 20 dB and a range of 37 dB have been demonstrated.

Techniques for increasing diffraction efficiency beyond the 10.1-percent limit of binary absorption holograms have been investigated. Ion milling has been used to produce 40-percent efficient, environmentally durable, all-glass holograms. Techniques for producing blazed, reflection holograms by anisotropic etching of silicon have also been explored. The further development of high-efficiency, large space-bandwidth product, e-beam computer generated holograms is expected to have a marked impact on the future of holographic optics.

Preface

This final technical report describes a three-year research program to investigate computer generated holograms written by electron beam lithography. This work was performed at Honeywell Corporate Technology Center under sponsorship of the Air Force Office of Scientific Research, Contract No. F4962[illegible]80-C-0029. The period of contract performance was from 1 January 1980 to 28 February 1983. The contract monitor has been Dr. John A. Neff, (former) program manager of Electronics and Material Science, AFOSR/NE. The principal investigator is Steven M. Arnold.

Abstract

This final report describes a three-year research program to investigate computer generated holograms produced by electron beam lithography. Because they are light weight and can create wavefronts of arbitrary complexity, computer generated holograms are attractive for applications such as optical data processing and optical testing. To be practical, these elements must have large space-bandwidth products, and have the qualities of high diffraction efficiency, low scattering, low aberration and low cost, as compared to conventional optics. We have developed generalized encoding algorithms and fabrication techniques for producing e-beam computer generated holograms having submicron feature sizes, distortion-free resolution of better than 0.4 micron, and space-bandwidth products in excess of 10^7. E-beam lithography is superior to optical plotting for writing computer generated holograms and, with further refinement, could be extended to produce holograms having space-bandwidth products as large as 10^{11}, comparing favorably with interferometrically recorded holograms.

We have demonstrated the application of e-beam computer generated holograms to the testing of asymmetric, aspheric optics having up to 123 waves of aspheric aberration. We have also developed an optical vector-matrix multiplication scheme that utilizes e-beam computer generated holograms to achieve high numerical accuracy and large numerical range; an accuracy of 20 dB and a range of 37 dB have been demonstrated.

Techniques for increasing diffraction efficiency beyond the 10.1-percent limit of binary absorption holograms have been investigated. Ion milling has been used to produce 40-percent efficient, environmentally durable, all-glass holograms. Techniques for producing blazed, reflection holograms by anisotropic etching of silicon have also been explored. The further development of high-efficiency, large space-bandwidth product, e-beam computer generated holograms is expected to have a marked impact on the future of holographic optics.

Table of Contents

Table of Contents (Concluded)

List of Illustrations

List of Illustrations (Continued)

List of Illustrations (Concluded)

List of Tables

Section 1
Introduction

Holographic optical elements can play an important role in many areas of optical engineering. Because they work by diffraction, they offer many advantages over conventional, refractive optical elements, most notably: compactness, light weight, and low replication cost. Against these advantages must be weighed their high dispersion (chromatic aberration) and limited diffraction efficiency.

Many research groups have demonstrated holographic optical elements in practical optical systems. Holographic lenses have been employed in interferometers, wherein they provide a reference wavefront for comparing optical surfaces [1-1]. They have also been used in laser machining to shape the laser [1-2]. In 1979, Fienup and Leonard [1-3] demonstrated that optical processors utilizing holographic optics were capable of processing images of large space-bandwidth product. More recently, Horner and Ludman [1-4] have shown the use of holographic optical elements for demultiplexing in fiber optic systems. To be more compatible with existing optical systems, these elements must have the qualities of low aberration, high diffraction efficiency over the desired field of view, low scattering, and low cost.

With ordinary interferometric recording of holographic optics, we are limited to the complexity and accuracy of available recording wavefronts, and also by the availability of suitable recording materials. If the recording and design wavelengths differ, creation of these recording wavefronts can become exceedingly difficult.

With computer generated holography, recording wavefronts are no longer necessary. The desired interference pattern is instead calculated and then plotted using a suitable graphic device. The advance of computer generated holography has opened a new frontier in holographic optics. It is by far the best technique for making optical elements to form wavefronts of arbitrary complexity.

Techniques for making binary computer generated holograms are well developed. Their potential in optical engineering applications is ever increasing. Computer generated holograms have been used in such areas as optical data processing, optical testing, optical memories, laser beam scanning, and 3-D image display. An article by W.H. Lee [1-5] is an excellent source of information on both the techniques of making computer generated holograms and their applications. With the development of improved fabrication techniques, more applications of computer generated holograms are anticipated in the future.

The computer generation of a hologram involves the following three major steps:

- Calculation of the complex wavefront at the hologram plane originating from a given wavefront at the object plane. For holographic lenses, this wavefront is

relatively simple and can usually be determined by ray tracing. For Fourier transform holograms, the calculation is considerably more complex, generally requiring calculation of the Fresnel-Fraunhoffer integral.

- Encoding of the analog wavefront into an equivalent digital representation. The Lohman technique and the Lee technique are the best-known encoding techniques. A binary representation of a holographic lens is shown in Figure 1-1.
- Fabrication of the hologram by translating the digital, mathematical representation to a suitable recording medium.

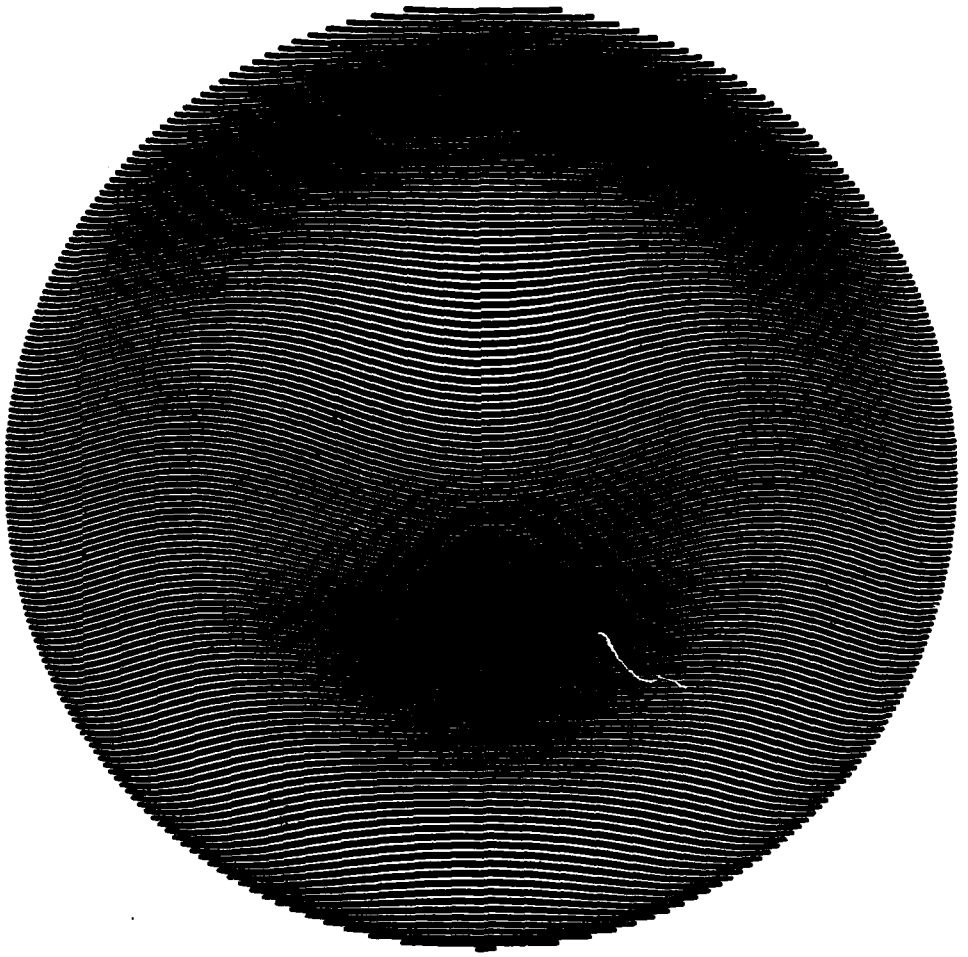

Figure 1-1. Example of a Binary, Computer Generated Hologram. A large grating period was specified in order to facilitate reproduction. The typical computer generated hologram would be much smaller and contain many more fringes.

The typical procedure for fabricating a computer generated hologram is to have the digitized interference pattern, which has been calculated and encoded by computer, drawn to a large scale by a computer-driven plotter. The drawing is then reduced photographically onto high-resolution film to the desired final size. There are several disadvantages and inherent limitations with this procedure: 1) errors are introduced in the plotting and photo-reduction processes; 2) optical plotting devices are limited in spatial resolution and space-bandwidth product, typically to 10^6 pixels; and 3) the turnaround time for the indirect procedure, from plotting to photo-reduction to film development, can be days, which is impractical for industrial applications.

Electron beam lithography overcomes all of the above disadvantages and limitations. E-beam writing of computer generated holograms is depicted in Figures 1-2 and 1-3. Distortion errors are significantly reduced because of direct writing and excellent spatial resolution. Figure 1-4 shows the submicron feature capability of holograms written by e-beam lithography. Holograms with linewidths as small as

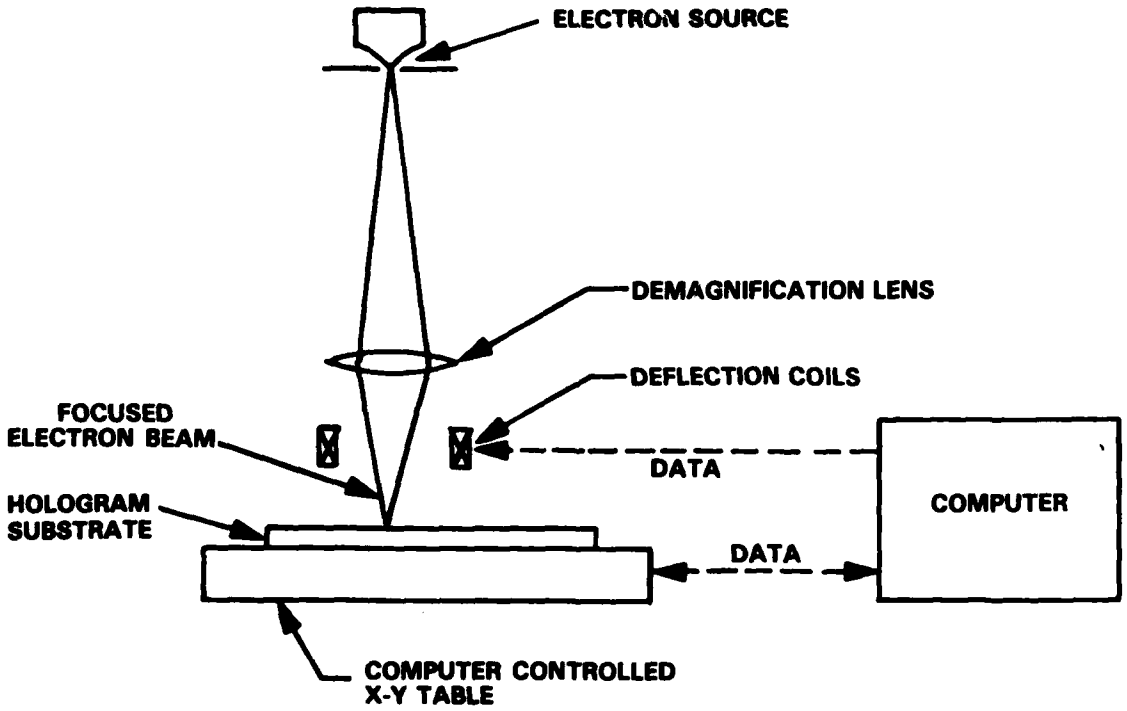

Figure 1-2. E-Beam Direct-Writing of a Computer Generated Hologram. The fringe pattern is created by a combination of beam deflections and workstage translations. Both are under control of the e-beam computer, which may also function to generate the fringe pattern data.

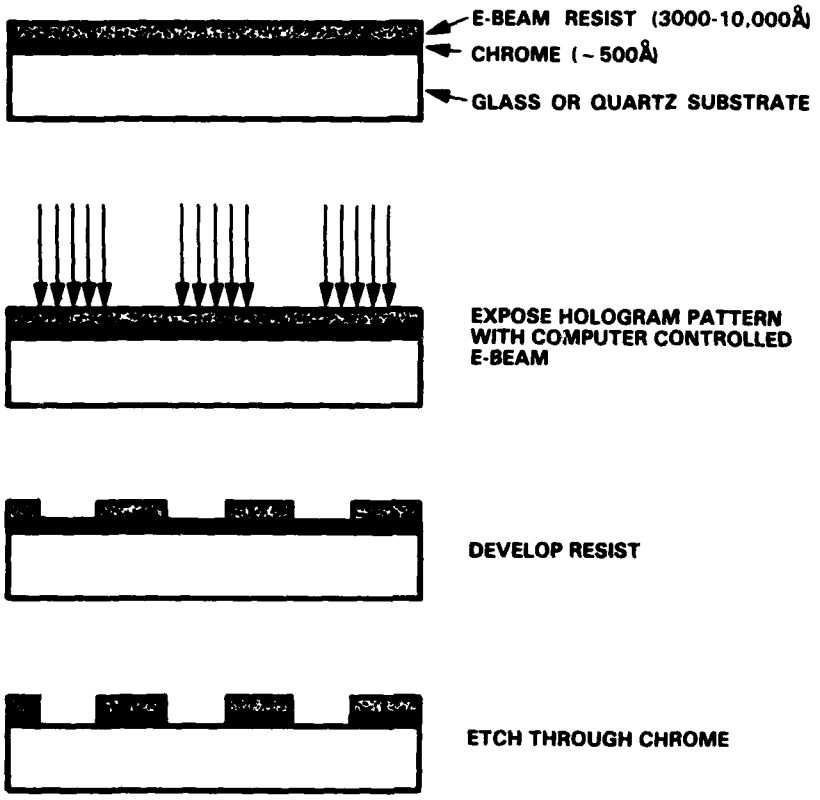

Figure 1-3. Fabrication Process for Binary, Chrome-on-Glass Type, Computer Generated Holograms. These holograms can have diffraction efficiencies of 10.1 percent.

1000Å have been demonstrated [1-6]. By comparison, the most advanced optical hologram writer can produce linewidths no narrower than 5 microns [1-7]. For e-beam computer generated holograms, the achievable number of pixels ($>10^{10}$) can approach that of interferometrically recorded off-axis holograms because of the sub-micron resolution and the capability of having many small scan fields (typically 1 mm x 1 mm) stitched together by interferometrically controlled translation of the workpiece. An advanced e-beam lithography system can easily produce a hologram directly onto a 3-inch substrate in 45 minutes, offering a much shorter turnaround time for practical applications when compared to indirect plotting.

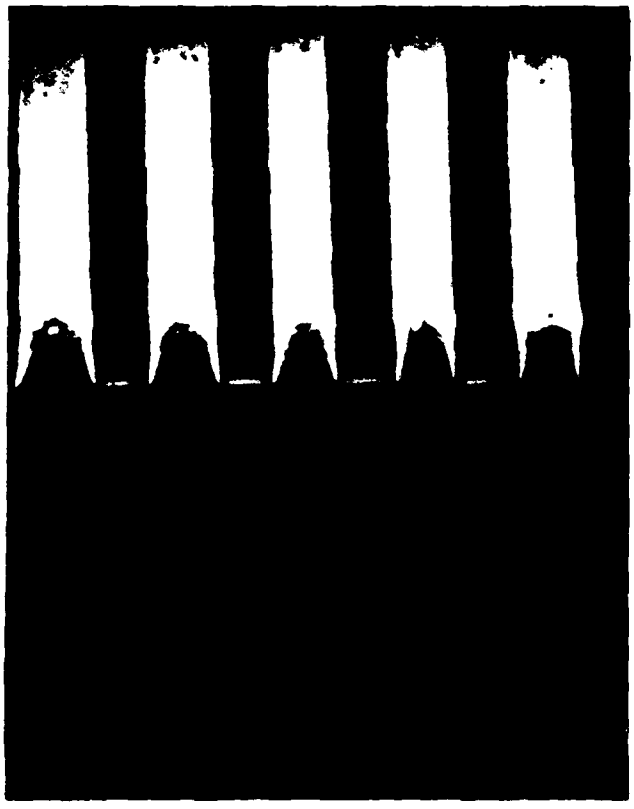

Figure 1-4. Grating Pattern in Honeywell-Proprietary Electron Resist EP25, as Produced by Honeywell's Cambridge EBMF E-Beam Lithography System. The grating period is 1.5 microns.

RESEARCH OBJECTIVES

The herein reported work under AFOSR Contract No. F49620-80-C-0029 initiated e-beam computer generated hologram research at Honeywell beginning on 1 January 1980.

Our overall long-range objective in this research has been to investigate and develop unique e-beam computer generated holograms, and to advance the fundamental knowledge of computer generated hologram technology for applications in optical research of current and future interest.

Our short-term objectives for the 1980 research program were:

- To evaluate the quality of e-beam writing
- To demonstrate the feasibility of using e-beam lithography to write high-performance computer generated holograms for use in aspheric testing.

Our initial efforts concentrated on evaluating the quality of e-beam writing using an existing Honeywell e-beam system and a plane wave interference technique. These studies not only advanced our understanding of making computer generated holograms by e-beam direct-writing, but also enabled us to improve our e-beam writing accuracy by software compensation. At the same time, we performed a distortion analysis of a state-of-the-art optical plotting device. The results of this analysis confirmed the superiority of e-beam lithography for writing computer generated holograms, and quantified the limitiations of indirect optical plotting techniques.

During the program, optimized software was developed to efficiently encode aspheric wavefronts of arbitrary complexity. We produced a computer generated hologram of an symmetric aspheric wavefront, designed to be tested using the Honeywell/Tropel holographic and shearing interferometer, thus demonstrating the feasibility of writing complex holograms by e-beam lithography. This technology has since been used to test aspheric diamond-turned optics at Honeywell's Electro-Optics Division.

As a continuation of our efforts to develop unique holographic optical elements using e-beam lithography, we proposed for 1981 to investigate and develop a new kind of hologram, the partitioned computer generated hologram (PCGH), which is useful in optical computing.

Our short-term objectives for the 1981 research program were:

- To analyze and develop capabilities for fabricating PCGHs using the unique capabilities of e-beam direct-writing.
- To demonstrate PCGHs applicable to optical computing, with maximum numerical range > 40 dB and maximum accuracy > 40 dB.

The PCGH differs from conventional computer generated holograms because it is spatially partitioned, fully uses available light by means of a space-variant illumination profile (such as a Gaussian distribution), and allows trimming for amplitude control. The unique capability of e-beam writing is especially useful to the PCGH.

During 1981, we developed an approach to the design of PCGHs, calculated achievable values of numerical range and accuracy, and implemented partitioning algorithms to produce PCGHs by e-beam lithography. We designed and fabricated PCGHs to perform the optical equivalent of a 1 x 10 matrix operation. In separate experiments, we encoded matrices with 20 dB of numerical accuracy and 37 dB of numerical range. These results were limited primarily by the stability of the laser light source.

Computer generated holograms are by far the best method for making optical elements to form wavefronts of arbitrary complexity, but their use has not been widespread. The reasons for this are several. They include limited space-bandwidth product, large computational effort, and low diffraction efficiency. We have shown that e-beam lithography can largely overcome the space-bandwidth limitation, and we

have demonstrated versatile and efficient encoding algorithms. As a continuation of our efforts to develop useful computer generated holograms using e-beam lithography, we proposed for 1982 to investigate and develop techniques for fabricating high-efficiency computer generated holograms.

Our short-term objectives for the 1982 proposed research program were:

- To analyze and develop techniques for fabricating e-beam computer generated holograms with diffraction efficiencies approaching 100 percent.
- To demonstrate high-efficiency, large numerical aperture, computer generated holograms capable of bringing a collimated He-Ne laser beam to a focus.

The diffraction efficiency of our chrome-on-glass computer generated holograms is limited to a theoretical maximum of 10.1 percent. We have investigated two approaches for achieving higher efficiency. The first approach involves ion milling of the hologram pattern into the glass to produce an all-glass, surface-relief type grating. Such a hologram is very environmentally durable and has a high damage threshold. We designed and fabricated several ion-milled holograms with diffraction efficiencies of 40 percent. While we had hoped to achieve 80-percent efficiency as grating periods approached a micron, difficulties in controlling linewidth in the thick resists prevented such gains.

Our second approach to high-efficiency computer generated holograms utilizes anisotropic etching to produce blazed grating patterns in silicon. We designed and fabricated a number of such blazed, crystalline holograms to either focus a plane wave or collimate a spherical wave. These holograms rely on sharply peaked groove profiles for their diffraction efficiency. Problems with undercutting of the etch mask adversely affected the groove profiles, preventing diffraction efficiencies in excess of about 20 percent.

Despite our limited success in fabricating them, we feel that e-beam produced surface-relief holograms have considerable potential.

The following sections report the program work in detail. Section 2 discusses the use of e-beam lithography in the writing of computer generated holograms, and presents our hologram encoding methods. Section 3 reports our application of e-beam computer generated holograms to problems of aspheric optical testing and optical vector-matrix multiplication. Section 4 reports our efforts to develop fabrication techniques for increased diffraction efficiency. Section 5 summarizes the program accomplishments.

REFERENCES

1-1 A.J. MacGovern and J.C. Wyant, "Computer Generated Holograms for Testing Optical Elements", Appl. Opt. *10*, 619-624 (1971).

1-2 N.C. Gallagher and D.W. Sweeney, "Infrared Holographic Optical Elements with Applications to Laser Material Processing", IEEE J. Quantum Electron. *QE-15*, 1369-1381 (1979).

1-3 J.R. Fienup and C.D. Leonard, "Holographic Optics for a Matched-Filter Optical Processor", Appl. Opt. *18*, 631-640 (1979).

1-4 J.L. Horner and J.E. Ludman, "Holographic Optical Element for Demultiplexing in Fiber Optic Systems", Proc. Soc. Photo-Opt. Instrumen. Eng. *215* (1980).

1-5 W.H. Lee, "Computer-Generated Holograms: Techniques and Applications", *Progress in Optics*, page 16, edited by E. Wolf, (North-Holland, Amsterdam, 1978).

1-6 D.C. Shaver, D.C. Flanders, N.M. Ceglio and H.I. Smith, "X-Ray Zone Plates Fabricated Using Electron-Beam and X-Ray Lithography", J. Vac. Sci. Technol. *16*, 1626-1630 (1980).

1-7 H.J. Caulfield, "National Computer Hologram Facility", private communication (1982).

Section 2
Electron Beam Fabrication of Computer Generated Holograms

Two essential requirements must be met to achieve a useful computer generated hologram. First, an adequate graphic device is needed for translating the conceptual and digital representation of the hologram into a recording medium. The graphic device must be capable of plotting hundreds of lines constructed from thousands of line segments to an accuracy of a fraction of the average line spacing. Commercially available optical recorders can provide only about 2000 x 2000 distortion-free pixels across the hologram. This is far below the 10^{10} or more pixels of a typical conventional hologram.

Second, adequate software is needed to drive the graphic device. The software will have to execute plotting procedures millions of times and must be efficient and flexible to economize the total plotting time. Preprocessing of data can reduce plotting time, but a compact data format is needed if data storage requirements are to be kept manageable.

Our overall objective in this program has been to extend the use of e-beam lithography to the making of computer generated holograms. In e-beam lithography, a highly collimated beam of electrons, under computer control, is used to expose a pattern in electron resist. The area over which the beam can be deflected with precision is limited (1 mm x 1 mm is typical) so that large patterns are made by translating the workpiece and stitching small pattern segments together.

Two approaches to the building of large patterns have been developed. One is where the workpiece is moved, brought to rest and the pattern segment exposed, usually in a vector-scan technique. The two lithography systems used in the present work were of this type. Early phases of the program used a Honeywell-developed electron beam exposure system (Honeywell EBES). Tests showed this instrument to be far superior to a state-of-the-art optical plotting device. In late 1980, Honeywell obtained an EBMF e-beam lithography system from Cambridge Instruments. Because of its superior resolution, this system soon supplanted the Honeywell EBES for hologram drawing.

A second approach to pattern composition is to keep the workpiece in continual motion while exposing a small stripe of the pattern in a raster-scan technique. Honeywell has recently acquired a system of this type, based on Bell Lab's EBES design.

This section discusses significant aspects of the Honeywell EBES and Cambridge EBMF e-beam lithography systems and compares e-beam lithography to optical plotting. Our hologram encoding methods are presented. The section concludes with a discussion of the capabilities and limitations of the Cambridge EBMF as a hologram writing tool.

HONEYWELL ELECTRON BEAM EXPOSURE SYSTEM (HONEYWELL EBES)

Honeywell initiated an e-beam lithography program in 1974 that included both system development and electron resist research. Figure 2-1 is a photograph of the Honeywell EBES system. In the following paragraphs, pattern distortion of the Honeywell EBES is discussed, comparison is made to a state-of-the-art optical recorder, and our hologram encoding method is presented.

Distortion Analysis

To demonstrate the feasibility of e-beam computer generated holograms, a prerequisite is to determine the distortion-free resolving power of the e-beam system. Then the system can be used to make holograms of predictable optical figure. Pattern distortion errors can have several sources. They include:

- Aberrations in the electron optics, particularly for large scan fields.
- Drift of the electron-optical axis due to contamination charging and stray fields.
- Drift in the deflection electronics.
- Deviations from flatness and orthogonality of the interferometer mirrors on the workpiece stage.
- Z-axis deviations due to workpiece positioning and warpage or stage misalignment.

Some of the distortions are reproducible and could, in principle, be compensated in the software; others are not. Typical positioning specifications of e-beam systems are ± 1/10 micron to ± 1/4 micron. There has been little independent verification of these specificatons. Distortion errors are most apparent when one attempts to draw a pattern which extends over more than one scan field. Lines which continue from one scan field to an adjacent scan field may fail to butt smoothly at the boundary between scans fields, leading to a pattern mismatch referred to as stitching error. When we began our work, a typical stitching error on the Honeywell EBES was ± 1 micron.

Our method of measuring e-beam pattern distortion is the interferometric technique introduced by Wyant [2-1]. The principle of this technique is simple. If an e-beam device is used to write a linear grating of straight, parallel lines, the resulting pattern can be thought of as a hologram produced by interfering two plane wavefronts. But, because of pattern distortion, the lines are never perfectly straight nor equally spaced. A pattern of distorted straight lines can be thought of as a hologram made by interfering a tilted plane wave with an aberrated plane wave. Experimentally, a Mach-Zehnder interferometer is set up to evaluate the aberrated plane wave. Once the interferogram is digitized and analyzed, a contour map for the entire pattern showing lines of constant distortion in a particular direction can be obtained. By combining two contour maps for distortion in orthogonal directions, the distortion in any arbitrary direction can be found.

E47069

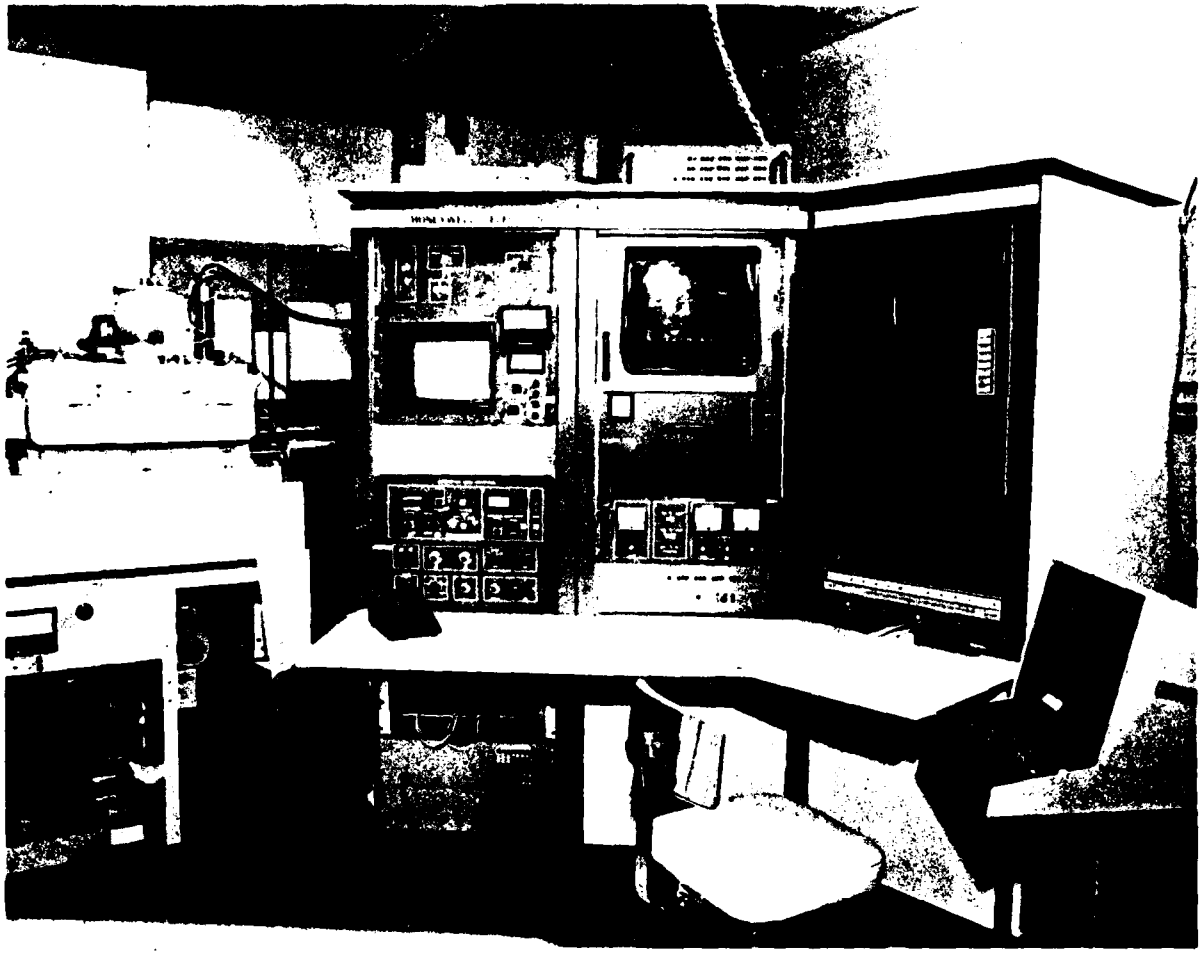

Figure 2-1. Honeywell's Electron Beam Exposure System (Honeywell EBES). At the left is the electron-optical column with a field emission source and electrostatic focusing. The scanning electron microscope electronics with CRT display are in the left rack, the interface electronics in the center rack and the minicomputer with core, disc and magnetic tape memory in the right-hand rack.

To perform the e-beam distortion analysis, we fabricated linear gratings and rectangular, crossed gratings. A crossed grating, as shown in Figure 2-2, allows orthogonal components of distortion to be tested with a single pattern. When the crossed grating is illuminated with a plane wave, several diffracted orders are produced as shown in Figure 2-3. An interferometer arrangement, as depicted in Figure 2-4, was used for interfering the +N and −N orders. Typical interferograms appear in Figure 2-5. A deviation from linearity of one fringe in the interferogram represents a pattern distortion of 1/2N grating periods.

As indicated earlier, our initial tests of the Honeywell EBES showed distortion errors of ± 1 micron. We took several steps toward reducing these errors:

- Scan field — the size was reduced to 1 mm x 1 mm from 1.6 mm x 1.6mm to minimize aberrations.
- Software compensation — the functional form of the distortions was fit to a nine-point polynomial and the coefficients were updated periodically during drawing to allow for temporal variations in the distortion. The coefficients were used to register the pattern to substrate marks as shown in Figure 2-6.
- Hardware improvements — some sources of magnetic interference were eliminated and special magnetic shielding was installed to reduce the effects of others.

These efforts brought us to the point where we could draw patterns with distortion errors of ± 0.15 micron in the X-scan and ± 0.30 micron in the Y-scan directions.

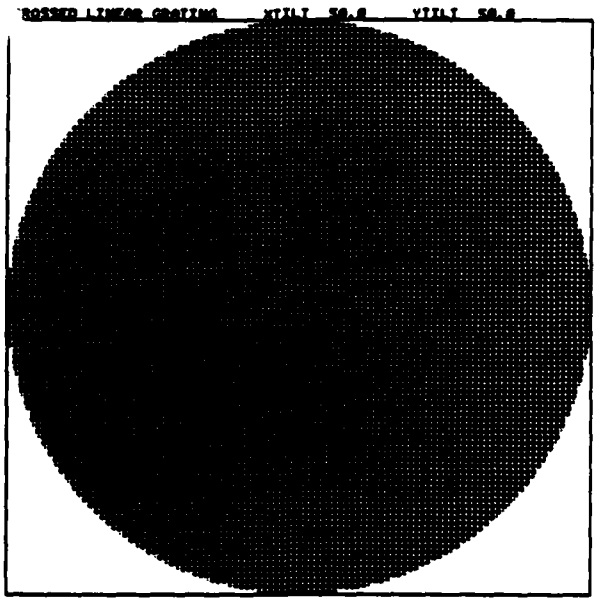

Figure 2-2. Rectangular Crossed Grating Used to Measure E-Beam Pattern Distortion

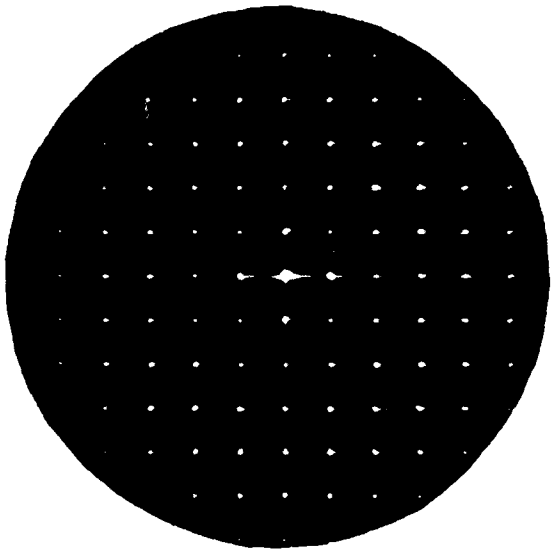

Figure 2-3. Diffraction Pattern of the Crossed Grating

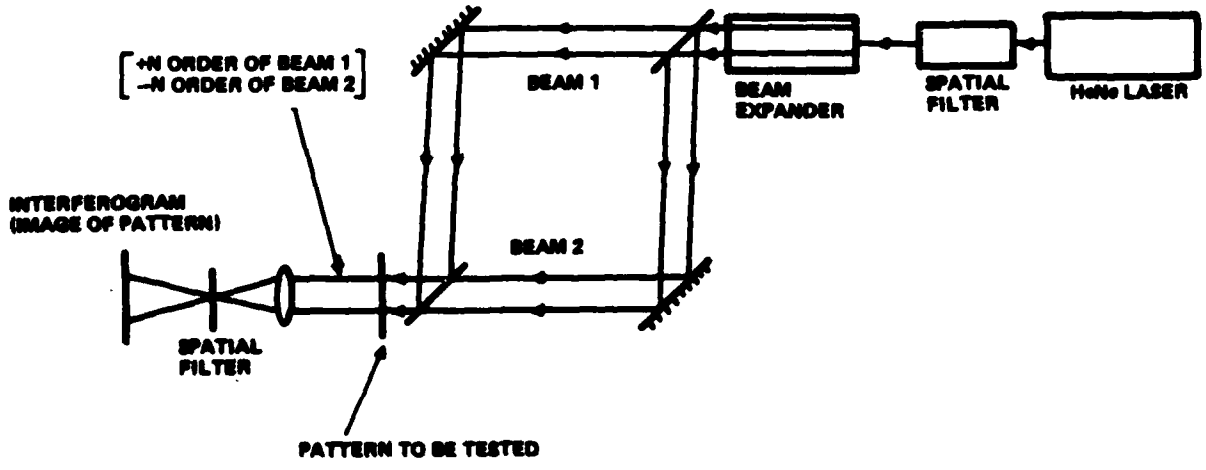

Figure 2-4. Interferometer Arrangement for Measuring E-Beam Pattern Distortion Using the Plane Wave Interference Technique

(a) Single scan field

(b) 2 × 2 multi-scan field

Figure 2-5. Distortion Tests of the Honeywell EBES. These typical interferograms are of linear gratings with a 5-micron period and 1mm × 1mm scan field size.

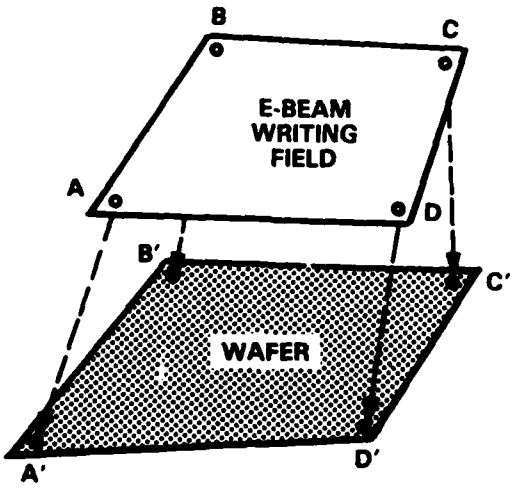

Figure 2-6. Software Distortion Correction. Aberrations in the electron optics are compensated by stretching the e-beam field.

Comparison with DICOMED Image Recorder

Conventionally, computer generated holograms have been drawn at large scale on a graphic plotting device and then photo-reduced to final size on high-resolution holographic film. Experience has shown that plotter distortion is one of the larger error sources in holograms produced by this method. In this research program, we sought to measure the limitations of the optical recording and photo-reduction method of hologram fabrication in order to assess the benefits of direct e-beam fabrication. We chose the DICOMED Image Recorder [2-2] as our optical recorder for this study.

Three crossed gratings of different spatial frequencies were plotted by the DICOMED Image Recorder each month for four consecutive months and then photo-reduced to a final size of 12 mm diameter. A distortion analysis was performed on these crossed gratings using the same testing technique as for e-beam writing. Figure 2-7 shows a typical interferogram from the crossed grating test using fourth orders (N = ± 4). This crossed grating had 200 lines per radius in each direction.

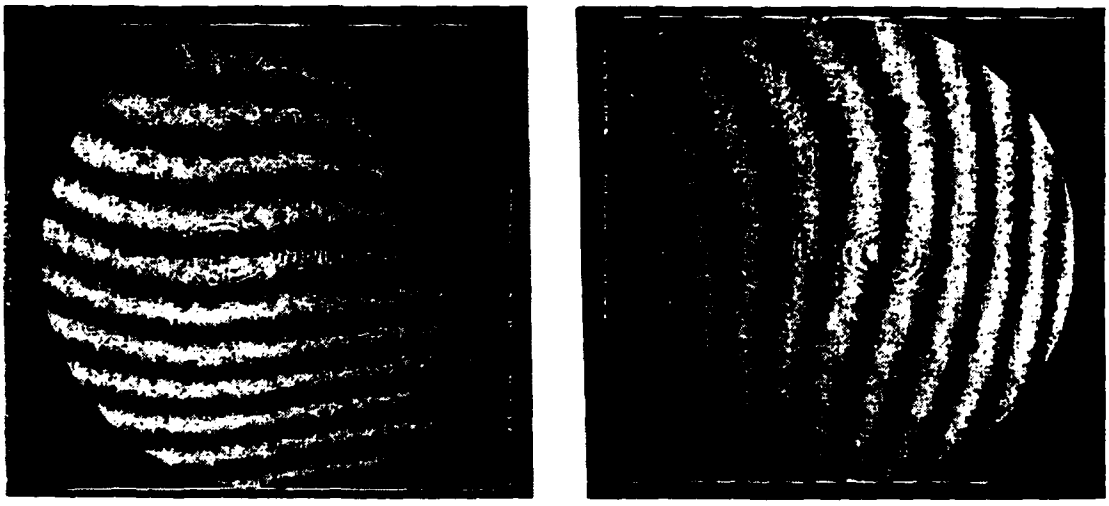

Figure 2-7. Distortion Test of the DICOMED Image Recorder. The interferograms were created using the N = ±4 orders of a crossed grating with 200 lines per radius. They show the components of distortion in orthogonal directions.

In this distortion analysis, we looked at three different aspects of the distortion errors:

- Distortion versus time (repeatability)
- Distortion versus polarity of the image
- Distortion versus photo-reduction process

In general, distortions in orthogonal directions had similar values. Plotting distortion did fluctuate from month to month within the six-month time frame, but stayed within the instrument specification of 0.25 percent. The dominant distortion was found to be astigmatism. Positive images had the least error. Measured errors included plotter distortion as well as lens distortion in the photo-reduction process. It was found that photo-reduction could contribute as much as 0.02-percent distortion error to the final hologram. The smaller the final size of the image, the larger the total distortion error.

We have concluded that the net pattern distortion for the DICOMED Image Recorder is less than 0.10 percent, with a usable resolution of 2000 elements per diameter. This can be used to encode wavefronts with a maximum slope of about 125 waves per radius, for which the maximum wavefront error would be 0.25 wave. By comparison, a 1 cm diameter e-beam generated pattern with $\pm$ 0.25-micron accuracy has 2×10^4 resolution elements per diameter and 0.01-percent distortion. This result confirms the benefits of e-beam fabrication of computer generated holograms.

Hologram Encoding Method

For simple wavefront holograms, only the phase need be encoded since the amplitude is constant over the entire hologram plane. Wyant and Bennett [2-3] plot wavefront holograms by drawing the centers of fringes formed by the conceptual interference between the desired wavefront and a tilted plane wave. In contrast to a Fourier transform hologram, the wavefront hologram generally has a simple functional form that can be quickly evaluated at any point on the hologram plane. Loomis [2-4] has extended this fringe-drawing method to calculate the phase of the wavefront at every pixel. For patterns of up to 4096 x 4096 pixels, this method uses reasonable amounts of computer time. For e-beam computer generated holograms, however, calculation of the wavefront at each pixel becomes prohibitive. We have therefore modified Loomis' method in order to develop software for producing practical e-beam computer generated wavefront holograms.

Our initial encoding method was geared toward the pattern generation capability of the Honeywell EBES. Since the Honeywell pattern generator was designed to efficiently expose arbitrarily oriented rectangular areas of a workpiece, we chose to represent a fringe by a series of connected rectangles of various sizes and orientations as depicted in Figure 2-8. A typical rectangle is perhaps 5 microns wide and 25 microns long. Since our pixel size is 0.3 micron, this means that one rectangle contains about 1400 pixels. Because only half of the pixels in a hologram are exposed, we can specify a hologram with 10^9 pixels by giving the locations of only 3.6×10^5 exposure rectangles. Each rectangle is specified by six numbers of 16 bits each. Therefore, a hologram can be specified by a total of 3.4×10^7 bits. Specification by Loomis' method would require 10^9 bits. Our encoding method therefore reduces the number of bits needed to specify a computer generated hologram by a factor of about 30.

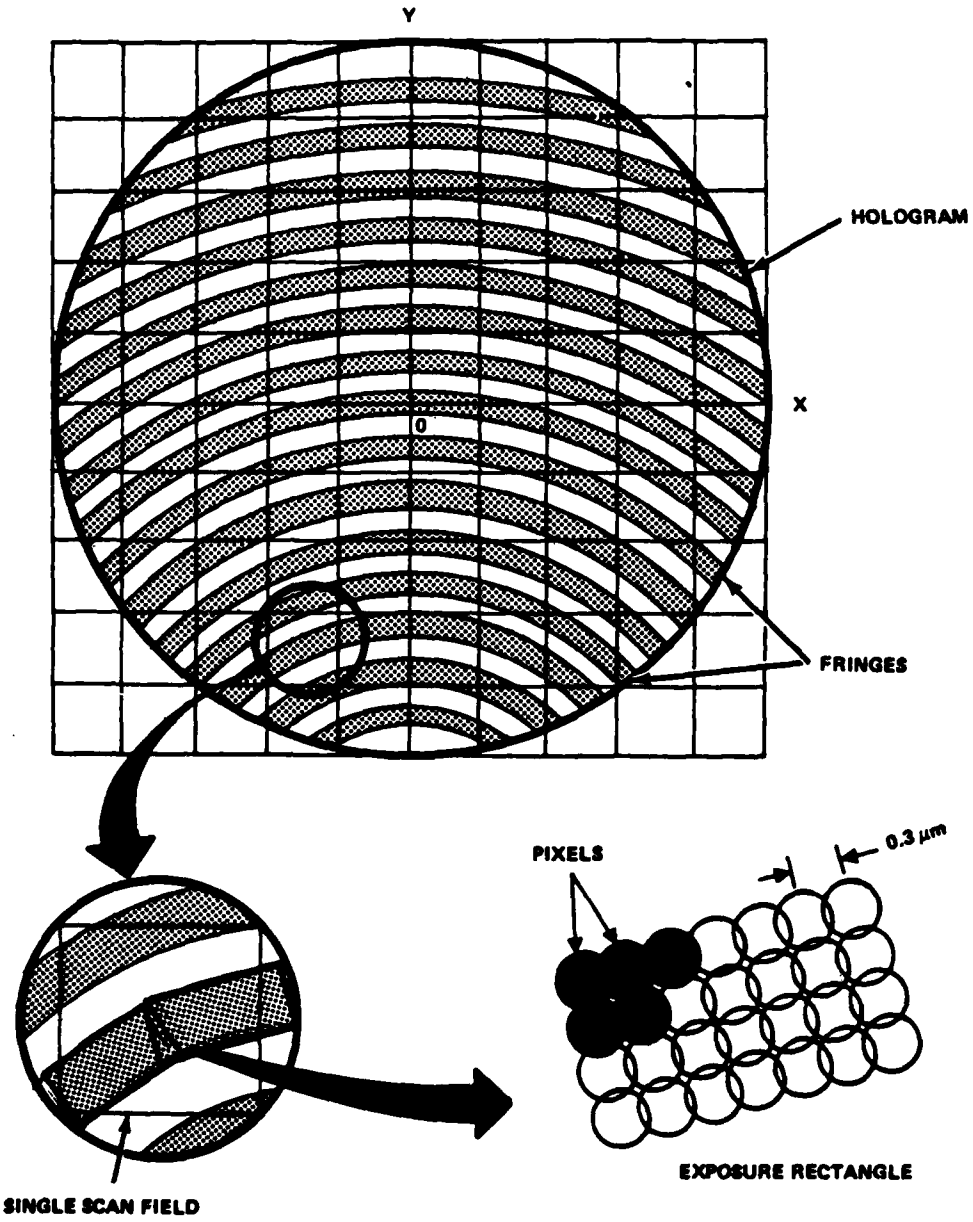

Figure 2-8. Hologram Encoding Method for Honeywell EBES. The pattern is *composed of rectangles in various orientations.* Each rectangle is an array of pixels on 0.3-micron centers. The exposure rectangle is the basic unit of data.

The bulk of our hologram encoding is performed during a preprocessing step on Honeywell's Multics computer system. The programs are written in PL1. A hologram is specified by its wavefront phase function $\phi(x,y)$. A subroutine must exist for evaluating this function. We are presently set up to handle functions of the form [2-5]

$$\phi(x,y) = \text{tilt} \times y + \frac{Cr^2}{1 + \sqrt{(1 - pC^2r^2)}} + a_2r^2 + a_4r^4 + a_6r^6 + a_8r^8 + a_{10}r^{10} + a_{12}r^{12}$$

where $r^2 = x^2 + (y - y_o)^2$. Other functional forms can easily be accommodated by replacing the subroutine.

Given a phase function $\phi(x,y)$, the program locates the centers of fringes as defined by the equation $\phi(x,y) = n$, where n assumes integer values. Fringes are traced across the hologram starting with the fringe of lowest n. The centerline of each fringe is approximated by a series of connected straight-line segments along which the phase $\phi(x,y)$ does not depart from its integer value by more than a specified amount, typically 0.05. Since the line segments are chosen to be as long as possible, this results in longer segments where the fringes are straight and shorter segments where the fringes have greater curvature. The program widens each line segment to form a rectangle, chosen so as to give a phase difference of 0.5 across the width.

Each rectangle is drawn as a square array of pixels, usually on 0.3 micron centers. This array is referred to as an exposure rectangle and is the basic unit of data accepted by the e-beam pattern generator. Exposure rectangles larger than a maximum size are partitioned into smaller rectangles prior to sorting into scan fields. A scan field consists of all rectangles that are to be drawn before repositioning the workpiece. Rectangles falling on a boundary are arbitrarily assigned to one of the scan fields they occupy. After sorting, the exposure rectangles are written to magnetic tape for reading by the e-beam computer.

A typical hologram of 10 mm diameter requires 88 scan fields and may contain nearly 2×10^5 exposure rectangles. It can be drawn in about 90 minutes.

CAMBRIDGE ELECTRON BEAM MICROFABRICATOR (EBMF)

In August of 1980, an EBMF-2 e-beam system from Cambridge Instruments was delivered to Honeywell's Solid State Electronics Division. Figure 2-9 is a photograph of this system. We interferometrically tested patterns of 5-micron linear gratings written by the EBMF. Multi-scan-field patterns having three different scan field sizes, 1 mm x 1 mm, 2 mm x 2 mm and 4 mm x 4 mm, were evaluated. All patterns had the same overall size of 8 mm x 8 mm. Obvious distortion, predominately pincushion effect, was observed in the 4 mm x 4 mm scan field pattern (Figure 2-10). For patterns drawn with a 1 mm x 1 mm scan field size (Figure 2-11), the pattern distortion was less than $\pm$ 0.2 micron. This corresponds to a writing accuracy of 0.004 percent over a 1-cm diameter image.

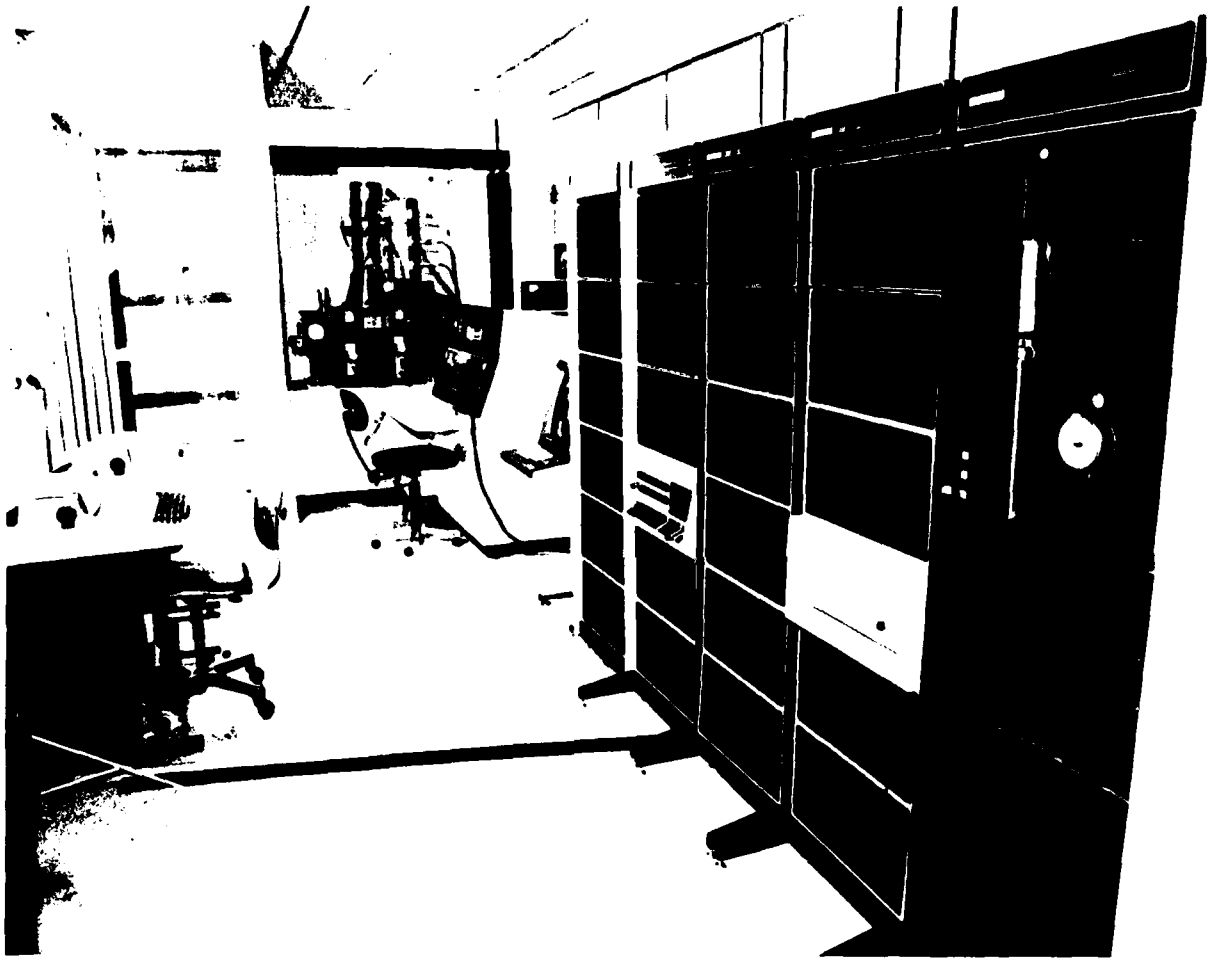

Figure 2-9. Cambridge EBMF E-Beam System. At the far end are the electron-optical column and operator's console. In the foreground are the system PDP11 computer and peripherals.

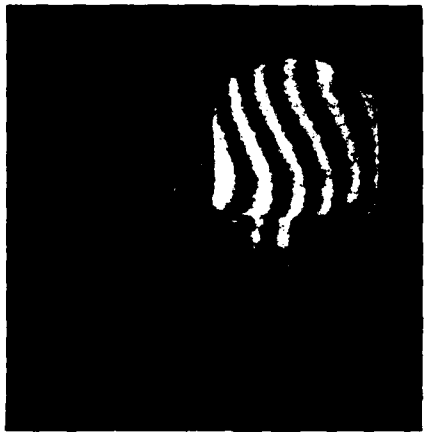

Figure 2-10. Distortion Test of the Cambridge EBMF E-Beam System with 4mm × 4mm Scan Field. The 8mm × 8mm pattern shows obvious distortion.

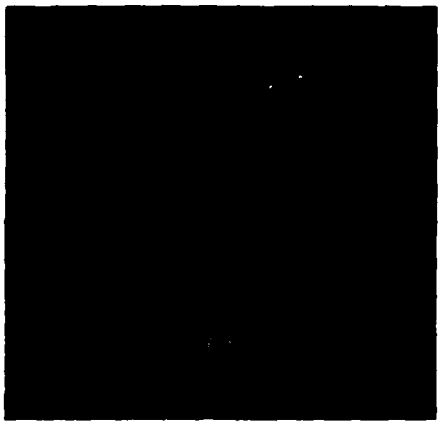

Figure 2-11. Distortion Test of the Cambridge EBMF E-Beam System with 1mm × 1mm Scan Field. The 8mm × 8mm pattern shows only 0.34-micron distortion.

Because of its superior writing accuracy (even without software compensation) and higher resolution, the Cambridge EMBF-2 soon supplanted the Honeywell EBES for writing of computer generated holograms. The Honeywell system has since been abandoned and the Cambridge system upgraded to an EBMF-6. The remainder of this section describes hologram fabrication with the EBMF-6.

Fabrication Procedure

Our current procedure for fabricating computer generated holograms with the EBMF involves several discrete steps:

- The hologram is encoded and written to magnetic tape in Cambridge source pattern data (SPD) format. This computation is performed on the Honeywell Multics computer system.
- The data is "fractured" into scan fields and converted to binary pattern data (BPD) for drawing. This step utilizes Cambridge software and runs on a PDP11 similar to the e-beam computer.
- The Cambridge EBMF is used to expose the hologram pattern in e-beam resist.
- After exposure and development, the pattern is either wet etched to produce a binary chrome-on-glass hologram or else ion milled to produce an all-glass binary phase hologram.

Hologram Encoding Methods

Our switch to the Cambridge EBMF for hologram writing required the development of new encoding algorithms. The reason for this is that, while the Honeywell EBES could draw rectangles of any orientation, the Cambridge machine is only capable of drawing rectangles at a few discrete angles. Consequently, we have developed several algorithms for reducing a hologram to a set of rectangles with horizontal and vertical sides. These algorithms, described below, can be compared on a basis of number of wavefront evaluations and amount of data storage required per hologram pixel. Here the term pixel refers to resolution actually utilized, which can be considerably less than the full distortion-free resolution available. Frequently, pixel size will differ in the two axes.

Poly Format — Our first encoding algorithm for the Cambridge EBMF is a direct adaptation of the previously described fringe-drawing method. Fringes are approximated by a series of points connected by straight-line segments. Standard Cambridge data-processing programs are then used to fracture the polygonal fringes into primitive shapes [2-6]. Poly format results in efficient, compact source code, as did the earlier algorithm from which it derives. Typical performance is 0.008 wavefront evaluations and 0.4 bits of source pattern data per hologram pixel. However, for any but the simplest holograms, subsequent fracturing consumes enormous amounts of computer time and produces prodigious quantities of binary pattern data that quickly fill all available storage devices.

Staircase Format — This encoding method can best be described by referring to Figure 2-12. Fringes are approximated by a number of rectangles with horizontal and vertical sides. The resulting "staircase" boundary is quite visible in regions where the fringes lie at significant angles to the scan axes. The staircase can be made as fine as 0.1 micron if one is willing to accept the penalty in size of data set. However, it is sufficient for the step size to be a small fraction (typically 0.05) of the fringe period, and steps are therefore made as large as possible while still satisfying this criterion. It is this ability to use large steps, and hence fewer rectangles, which constitutes the principle advantage of Staircase format. Fracturing to binary pattern data is quicker than for Poly format and actually reduces the size of data set. Defining pixel size as the scale of the staircase boundary (variable across the hologram),

Figure 2-12. STAIRCASE Encoding Method for Cambridge EBMF. The rectangle is the basic unit of data. Only four rectangle orientations are allowed, hence the stepped pattern.

Staircase format requires about 0.1 wavefront evaluation and 12 bits of source pattern data per hologram pixel.

Raster Format — The motivation for this third encoding method is to produce fractured binary pattern data directly and/or to produce data for our raster-scan machine. The Raster encoding method abandons fringe tracing and instead proceeds scan field by scan field and pixel by pixel. Pixel size is fixed on the basis of space-bandwidth requirements, but generally exceeds the 0.1 micron e-beam address resolution. A typical pixel size is 0.4 micron by 3.2 microns. The Raster algorithm is not yet fully implemented, in that wavefront evaluation occurs at every pixel and the output is still in Cambridge SPD format. Because of its fixed pixel size, this algorithm, even when using run-length encoding, produces somewhat more source pattern data than the Staircase algorithm.

Present Capabilities and Limitations

The capabilities and limitations of the Cambridge EBMF as a hologram writing tool are summarized below. Staircase encoding format is assumed.

Linewidth and Pattern Accuracy — At present, we are capable of routinely fabricating e-beam computer generated holograms with spatial accuracy (distortion-free resolution) of 0.4 microns. Line widths of 1 micron are readily achievable, and narrower lines are probably not useful without improved pattern accuracy.

Wavefront Specification — The Staircase encoding algorithm will accept any wavefront $\phi(x,y)$ having sufficient tilt to assure $\partial\phi(x,y)/\partial y > 0$.

Maximum Hologram Size — Hologram size is essentially data-limited. Staircase format allows about 4×10^5 exposure rectangles per reel of magnetic tape. This is enough to encode holograms having $4 \times 10^5/\Delta\phi$ pixels, where $\Delta\phi$ is the desired wavefront accuracy ($\Delta\phi = 0.05$ typical). A typical hologram is 10 to 12 mm in diameter, contains 300 to 400 fringes, and fills most of 1 reel of tape. Workstage travel places an absolute upper limit of 100 mm × 100 mm on hologram size.

Diffraction Efficiency — Efficiencies near the theoretical maximum of 10.1 percent for binary absorption holograms and 40.5 percent for binary phase holograms are attainable.

Fabrication Time — Turnaround time is limited primarily by e-beam availability and varies from 1 day to several weeks. Actual fabrication time is typically 30 minutes to encode, several hours to fracture, 45 minutes to expose, and 30 minutes to develop and ion mill. The exposure-limited writing speed of the EBMF is 0.02 to 1.0 cm^2/min, depending on required resolution.

Potential for Further Improvement

Significant potential exists for increasing the hologram writing capability of the EBMF e-beam through software improvements. At present we are severely data-limited. Cambridge SPD format requires about 12 bits per hologram pixel; this is clearly excessive. Fracturing time could be eliminated and data quantity halved by generating BPD format data directly on Multics. Generating data directly on the e-beam's PDP11 as exposure proceeds might eliminate the data bottleneck entirely. Software distortion correction could improve the spatial accuracy to 0.2 microns.

The Cambridge e-beam's pattern generation capability is not well suited to the fringe drawing method of hologram generation. In general, commercially available vector-scan e-beam systems are aimed toward sparse, rectilinear patterns, while raster-scan systems sacrifice resolution (0.5 to 1.0 micron typical) for drawing speed.

If the data problem was overcome, perhaps by converting to raster scanning and generation of data while drawing, a higher resolution e-beam such as the EBMF could likely provide 0.2-micron spatial accuracy over a 10 cm × 10 cm area with a drawing speed of 1 cm^2/min. This would correspond to a space-bandwidth product, or distortion-free pixel count, of 2.5×10^{11} which compares favorably with interferometrically recorded holograms.

REFERENCES

2-1 J.C. Wyant, P.K. O'Neill and A.J. MacGovern, "Interferometric Method of Measuring Plotter Distortion," Appl. Opt. *13*, 1549-1551 (1974).

2-2 *The DICOMED D47 Image Recorder Operation and Programming Manual*, Dicomed Corporation, Minneapolis, Minnesota (1976).

2-3 J.C. Wyant and V.P. Bennett, "Using Computer-Generated Holograms to Test Aspheric Wavefronts," Appl. Opt. *11*, 2833-2839 (1972).

2-4 J.S. Loomis, "Computer-Generated Holography and Optical Testing," Proc. Soc. Photo-Opt. Instrumen. Eng. *215* (1980).

2-5 W.J. Smith, *Modern Optical Engineering*, page 257, (McGraw-Hill, New York, 1966).

2-6 P.G. Flavin, "Fabrication of Curved Structures by Electron-Beam Lithography," Electron. Lett. *18*, 865-876 (1982).

Section 3
Applications

Our second main objective, after having demonstrated the feasibility of e-beam computer generated holograms, has been to demonstrate useful applications of these optical elements. We have demonstrated applications in two major areas: optical testing and optical computing.

We have developed an aspheric optical testing capability utilizing e-beam computer generated holograms. This technology has been used to provide routine testing of aspheric diamond-turned optics at our Electro-Optics Division. We have also developed a scheme for optical vector-matrix multiplication which utilizes an e-beam generated holographic mask. This approach results in a fairly simple optical system offering both large numerical range and high accuracy. Simple holographic masks have been fabricated and tested.

In the remainder of this section, we describe in detail our application of e-beam computer generated holograms to both aspheric optical testing and optical vector-matrix multiplication.

ASPHERIC OPTICAL TESTING

The high performance and low cost requirements of modern optical systems demand the frequent use of aspheric surfaces and thus the ability to test these surfaces. Often, aspheric testing is impossible when conventional master surfaces are used as test plates. Therefore, deep aspheric surfaces are usually avoided by optical designers. This problem can be alleviated by storing the desired aspheric wavefront in the form of a computer generated hologram [3-1, 3-2, 3-3]. This stored wavefront can later be used in the interferometric testing of supposedly identical aspheric optical elements, much as a test plate is used in the conventional testing of spherical optical elements.

The Honeywell/Tropel interferometer used in this work is a custom designed instrument capable of testing aspheric surfaces using computer generated holograms. Figure 3-1 shows the physical appearance of this interferometer. Figure 3-2 is an exploded view depicting all the optical elements. Basically, the instrument is a Twyman-Green interferometer in which both the aspheric test beam and the spherical reference beam pass through the hologram. The first-order reference beam and zero-order (undiffracted) test beam are then combined to produce an interference pattern. Much of the apparent complexity results from the use of high-efficiency polarizing beam splitters. A detailed description of this interferometer is given elsewhere [3-4].

To illustrate the procedure for using e-beam computer generated holograms to test aspheric optics, we use, as an example, the testing of a 4-inch diameter f/2 parabolic

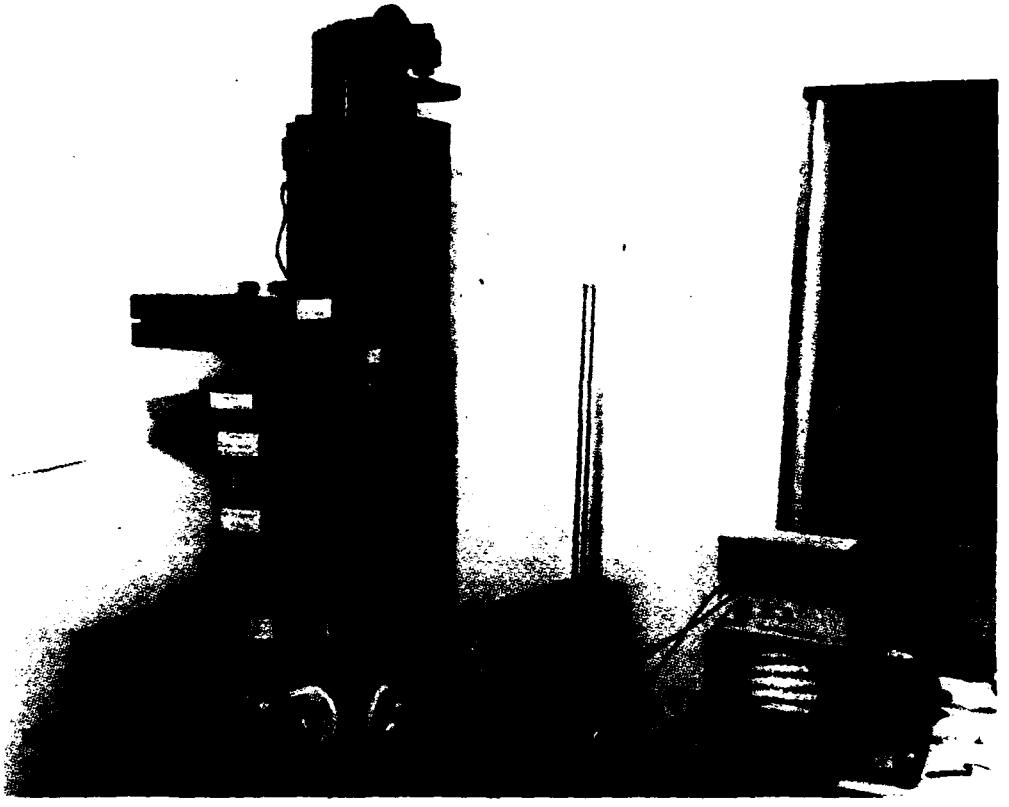

Figure 3-1. A Photograph of the Honeywell/Tropel Holographic and Shearing Interferometer in Operation

mirror [3-5]. A second example of a tilted plane-parallel plate will then demonstrate the capability of testing deep aspheric optics lacking rotational symmetry.

Example 1: 4-inch Diameter f/2 Parabola

The procedures involved in the testing of the f/2 parabola are as follows:

Step 1 — A mathematical description of the f/2 parabola is used in a ray tracing program along with the optical design data for the interferometer. The computer calculates the best position for the parabola, and also the fringe pattern that would be produced at the hologram plane if a perfect test wavefront were interfered with a reference wavefront at a particular non-zero incident angle. Known imperfections in the interferometer optics can be compensated for in the ray tracing.

Step 2 — The mathematical description of the fringe pattern is used to encode and fabricate an e-beam computer generated hologram using the methods discussed in the previous section. The finished hologram and its diffraction pattern are shown in Figures 3-3 and 3-4.

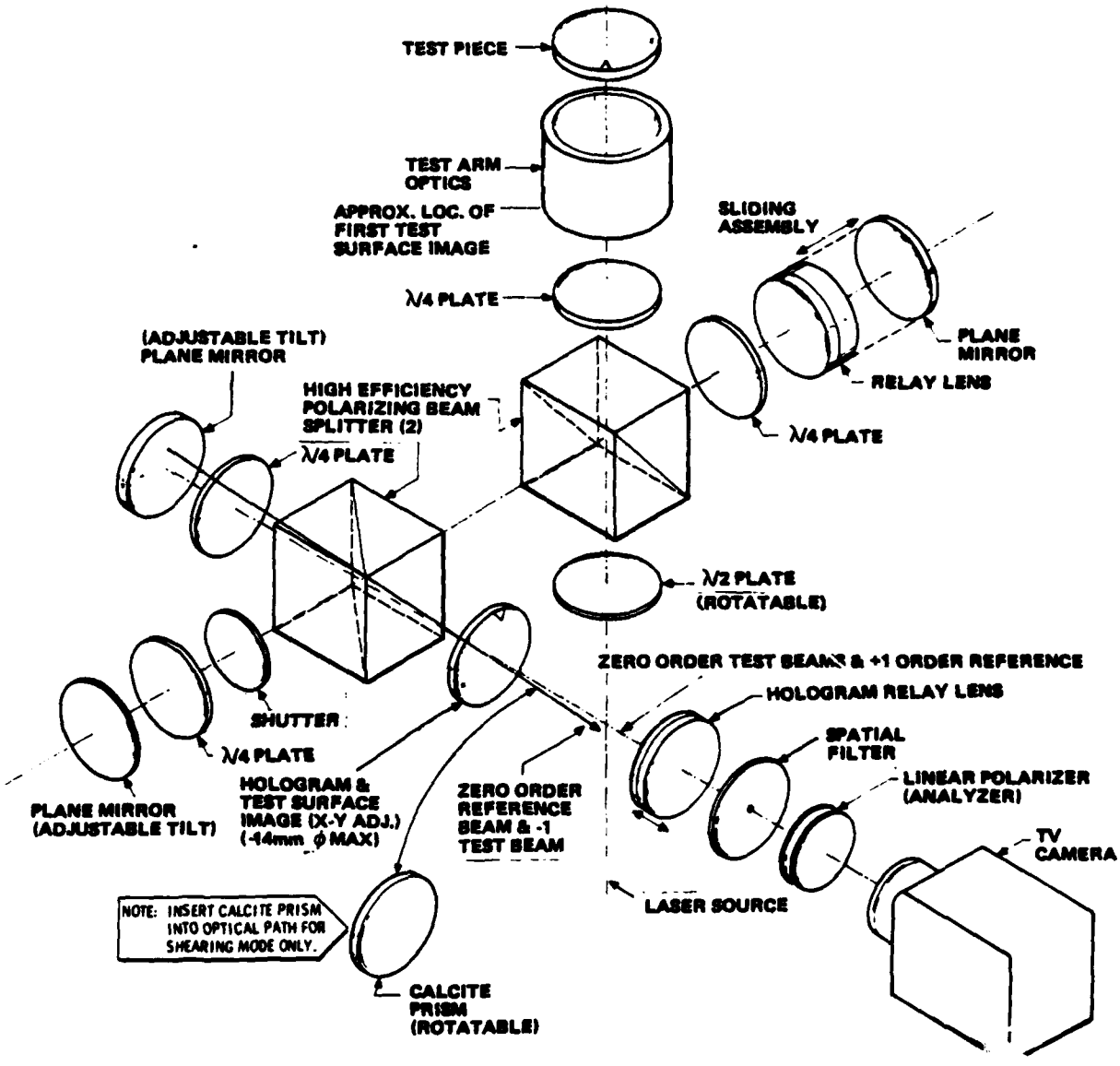

Figure 3-2 An Exploded View of the Honeywell/Tropel Holographic and Shearing Interferometer Showing All the Optical Elements

Figure 3-3. E-Beam Computer Generated Hologram for Testing of the f/2 Parabolic Mirror

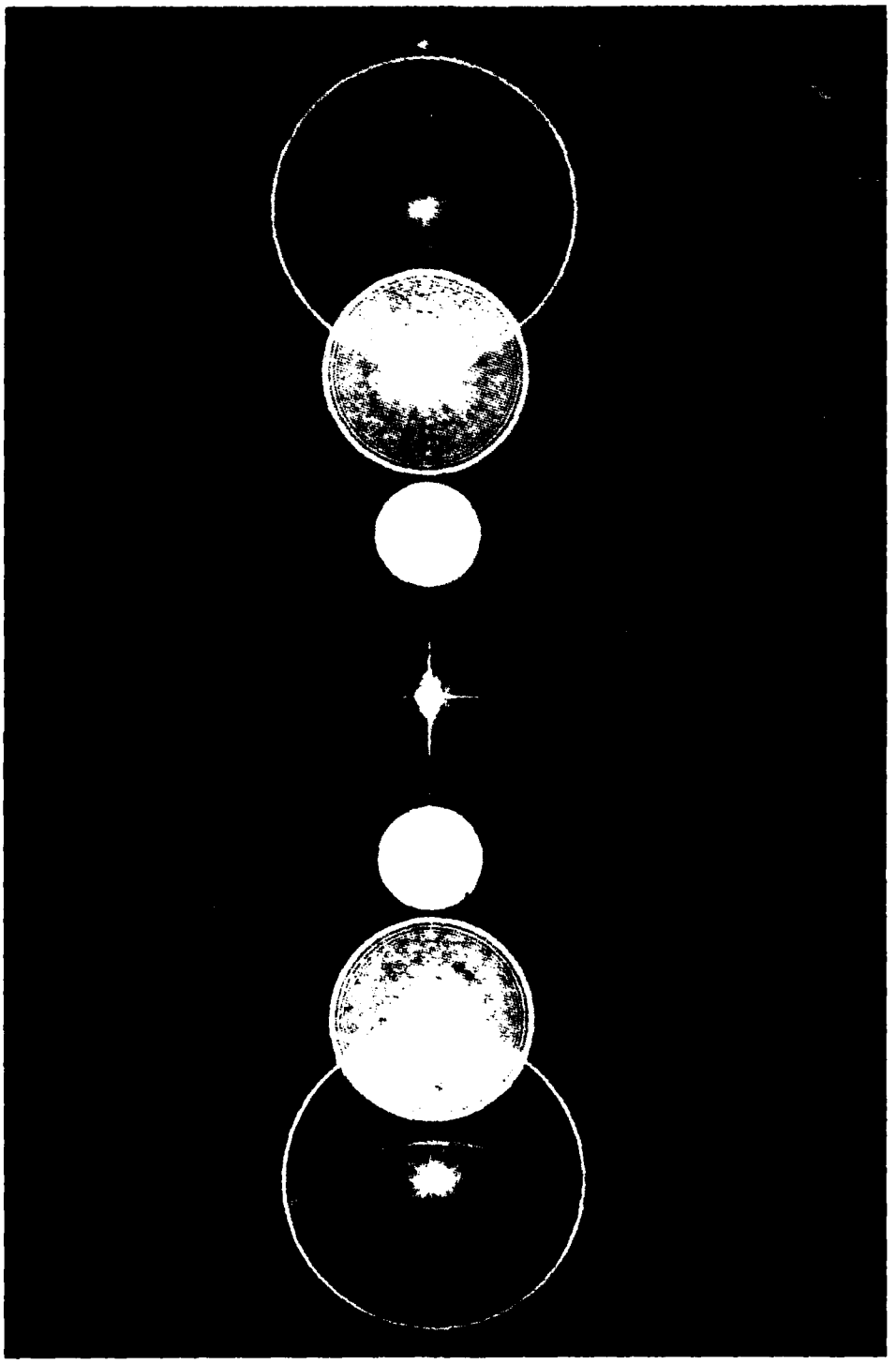

Figure 3-4. Diffraction Pattern Due to the Hologram of Figure 3-3.

Step 3 — When the finished e-beam computer generated hologram is inserted properly at the hologram plane of the interferometer system, both the test beam and the reference beam are diffracted by the hologram into plus and minus first-order beams. When the zero-order test beam and the zero-order reference beam are superimposed, the f/2 parabola is tested without aid of the computer generated hologram, and the interferogram of Figure 3-5a results. It shows about 40 waves of spherical aberration. This Twyman-Green interferogram would be exceedingly difficult to analyze in detail. However, its complexity is incorporated into the hologram, as shown by the interferogram in Figure 3-5b. This latter interferogram, produced by interfering zero and first orders of a reference beam, simulates the Twyman-Green test of a perfect f/2 parabola with compensation for known instrumental errors. When the reference beam is properly adjusted, the first-order reference and the zero-order test beams can be superimposed to produce the interferogram of Figure 3-5c. This interferogram gives the residual wavefront error of the f/2 parabola. If the parabola were perfect, the fringes would be straight, parallel and equally spaced. For comparison, the results of an autocollimation test are shown in Figure 3-6. The two tests are in good agreement.

Example 2: Asymmetric Deep Aspheric

The f/2 parabola test demonstrated the feasibility of using e-beam computer generated holograms to test known conic surfaces of moderate asphericity. For our second example, we designed an asymmetric deep aspheric wavefront using a concave mirror and a tilted plane-parallel plate as the test surface. Figure 3-7 shows the experimental setup used to obtain this wavefront. The amount of aspheric aberration in this wavefront can be selected by tilting the plane-parallel plate placed between the concave mirror the the diverger. Table 3-1 lists wavefront aberration as a function of parallel plate tilt angle.

Based on the coefficients obtained from ray tracing, we fabricated e-beam computer generated holograms to test this aspheric wavefront. This required a departure from our normal parametric description, but the change was easily accommodated because of the modularity of our encoding software. Holograms were generated corresponding to parallel plate tilt angles of 20 and 25 degrees. The rather unusual diffraction patterns of these holograms are shown in Figures 3-8 and 3-9.

Figure 3-10 is a Twyman-Green interferogram of the test wavefront with a plate tilt angle of 20 degrees (analogous to Figure 3-5a for the f/2 parabola). Figure 3-11 shows the e-beam computer generated hologram test of this asymmetric, aspheric wavefront. This test clearly demonstrates the capability of testing generalized aspheric surfaces with e-beam computer generated holograms.

E47069

a) Twyman-Green interferogram of the 4-inch diameter f/2 parabola

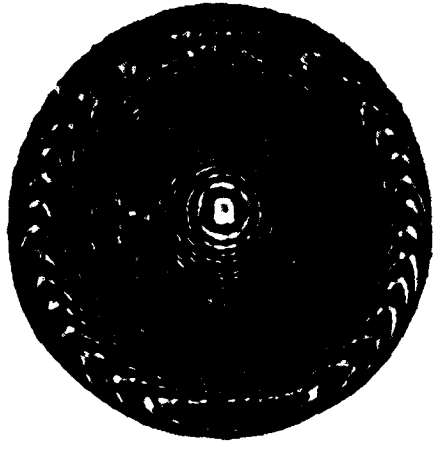

b) Interferogram of 12mm diameter e-beam computer generated hologram to simulate a perfect f/2 parabola and to compensate for instrumental error.

c) E-beam computer generated hologram test of the f/2 parabola. Surface deviation at 6328Å is 0.03 waves rms, 0.14 waves pv.

Figure 3-5. Testing of the f/2 Parabola with an E-Beam Computer Generated Hologram

Figure 3-6. Autocollimation Test of the f/2 Parabola. Surface deviation at 6328Å is 0.035 waves rms, 0.171 waves pv.

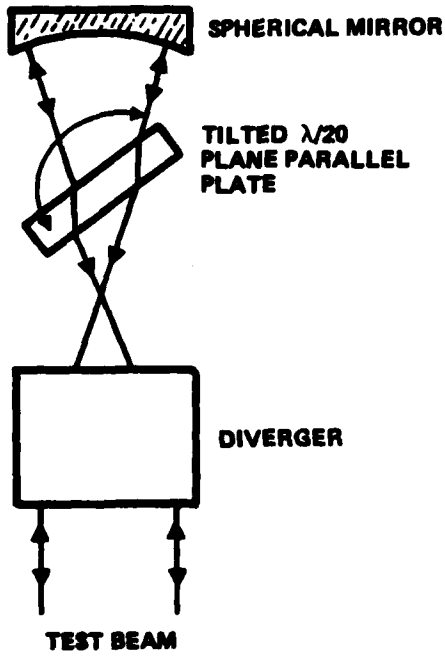

Figure 3-7. Experimental Arrangement to Obtain Asymmetric Aspheric Wavefront

Table 3-1. Asymmetric Aspheric Wavefronts

Tilt Angle	Slope (Waves/Radius)
15°	71
17.3°	83
20°	97
25°	123

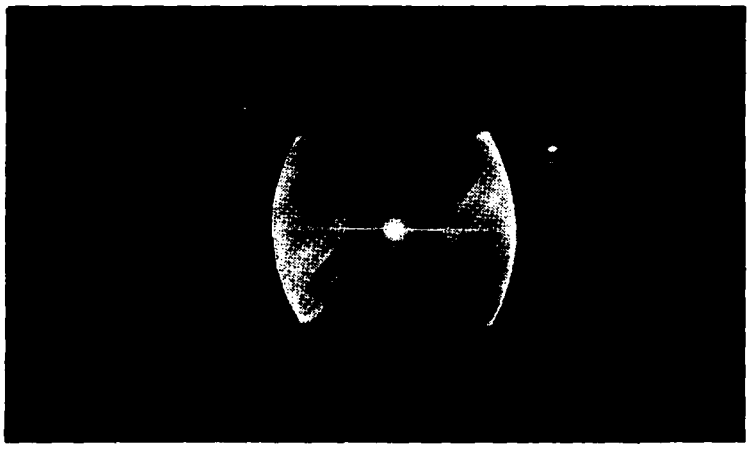

Figure 3-8. Diffraction Pattern of E-Beam Computer Generated Hologram to Simulate Asymmetric Aspheric Wavefront for Plate Tilt Angle of 20 Degrees

Figure 3-9. Diffraction Pattern of an E-Beam Computer Generated Hologram to Simulate Asymmetric Aspheric Wavefront for Plate Tilt Angle of 25 Degrees

Figure 3-10. Twyman-Green Interferogram of Asymmetric Aspheric Wavefront for Plate Tilt Angle of 20 Degrees

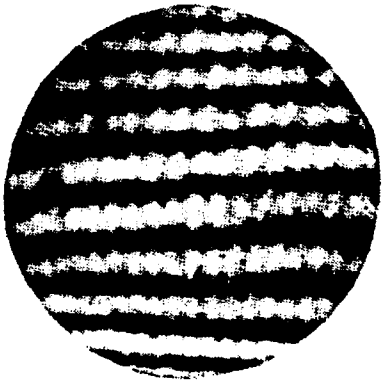

Figure 3-11. E-Beam Computer Generated Hologram Test of Asymmetric Aspheric Wavefront for Plate Tilt Angle of 20 Degrees. Surface deviation at 6328Å is 0.04 waves rms, 0.29 waves pv.

OPTICAL VECTOR-MATRIX MULTIPLICATION

There has recently been considerable interest in optical computing since it offers very high computation throughput rates for mathematical operations amenable to parallel computation. One class of such operations, vector-matrix multiplication with a fixed matrix, can be used for performing discrete Fourier transforms, coordinate transformations, pattern classification, and many other computations [3-6, 3-7, 3-8, 3-9, 3-10]. The general matrix-vector multiplication may be written as:

$$y_m = \sum_{n=1}^{N} H_{mn} x_n \qquad (m=1, 2, \ldots M)$$

Our optical approach to performing this computation uses N light sources to represent the components of x_n of the input vector, M detectors to represent the components of y_m of the output vector, and suitable optics to assure that a fraction H_{mn} of the light from source x_n gets to each detector y_m. The problem can be suitably scaled so that all parameters fall within acceptable positive ranges. Optics to perform the function of the matrix H remain fixed, while the N sources are modulated to represent various input vectors x.

In principle, the performance of this optical computer is dependent on a number of considerations involving the optics, detectors and sources. In practice, accuracy is often limited by matrix mask imperfections, while speed is limited by the amount of light reaching the detectors. For this reason, our work has focused on efficient optics to precisely distribute light among the various detectors.

In most schemes for optical vector-matrix multiplication, the matrix is encoded as a rectangular array of apertures or gray tones in a mask. This approach, represented in Figure 3-12, encounters several limitations. A complicated optical system is required in order to illuminate and receive light from specific columns and rows of the matrix mask. Much light is discarded in providing uniform illumination to the mask, with the mask passing only about half of what remains. Numerical range and accuracy are limited by the space-bandwidth product of the mask (generally less than 10^6 with conventional plotting techniques). Small matrix elements result in small apertures with low relative accuracies. If results differ from those intended, it is generally difficult to modify a mask except by starting anew.

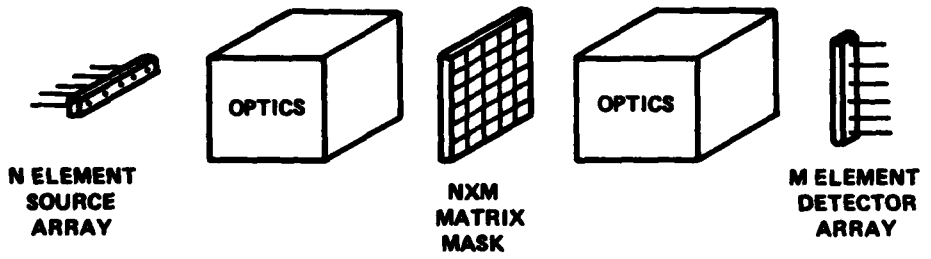

Figure 3-12. A general scheme for Optical Vector-Matrix Multiplication

PCGH Configuration

Our approach to optical vector-matrix multiplication, depicted in Figure 3-13, is based upon an e-beam generated diffractive mask which we will call a partitioned computer generated hologram or PCGH [3-10]. Each of N PCGHs is illuminated by collimated light from a single element of the source array and thus represents one column of the NxM matrix mask in Figure 3-12. Each PCGH is partitioned into M linear gratings, which diffract light to the M detectors. The optical power diffracted

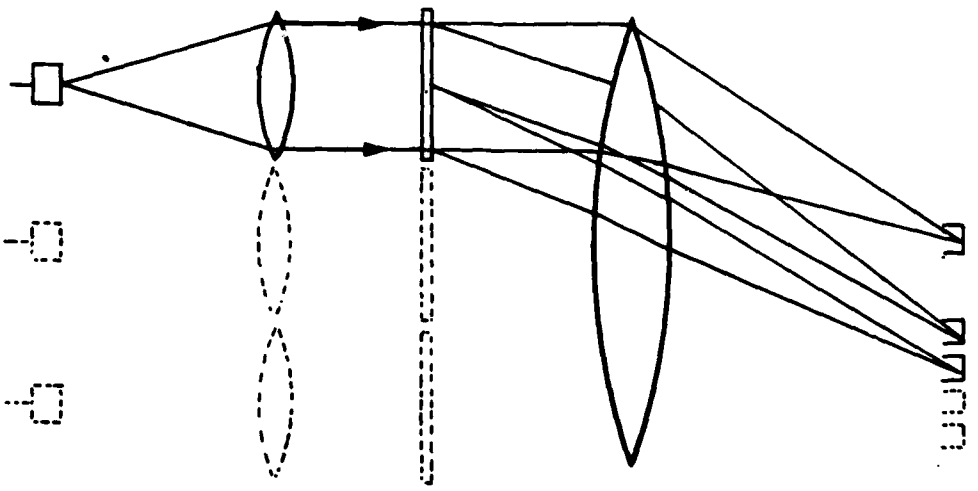

Figure 3-13. Partitioned Computer Generated Hologram (PCGH), Vector-Matrix Multiplier. The several facets of each PCGH contain linear gratings that deflect portions of the light to the various detectors.

by a particular grating is made proportional to the value of the required matrix element. The PCGHs are fabricated as binary chrome-on-glass holograms with the grating pattern delineated via e-beam lithography.

Our e-beam PCGH vector-matrix multiplication scheme has several advantages over the scheme in Figure 3-12. E-beam lithography offers a higher space-bandwidth product, which can translate into greater numerical accuracy. Also, the PCGHs are in the Fourier plane of the tranform lens with respect to the detectors. This means that the only requirement for light to reach a particular detector is that it be traveling in the proper direction upon leaving the PCGH. Therefore, each input module, consisting of source, collimating lens and PCGH, may be located anywhere within the aperture of the transform lens. This same immunity to translation allows a PCGH to be partitioned into facets in any manner consistent with dividing up the available light amongst the various detectors (providing, of course, that the facets do not become too small). Other advantages relate to optical efficiency. Except for diffraction efficiency losses, all light striking the PCGH can be used. Light need not be wasted in achieving uniform illumination; non-uniform illumination is acceptable so long as its effects are accounted for in the partitioning. Small facets associated with lesser outputs can be made physically larger by placing them where PCGH illumination is lowest. The various considerations which affect the design of a PCGH are discussed in the following sections.

PCGH Diffraction Analysis

Figure 3-14 illustrates a simple PCGH intended to produce 10 equal intensity outputs when uniformly illuminated. This PCGH has 10 equal area facets, each containing a linear grating to diffract incident light to the appropriate detector. The

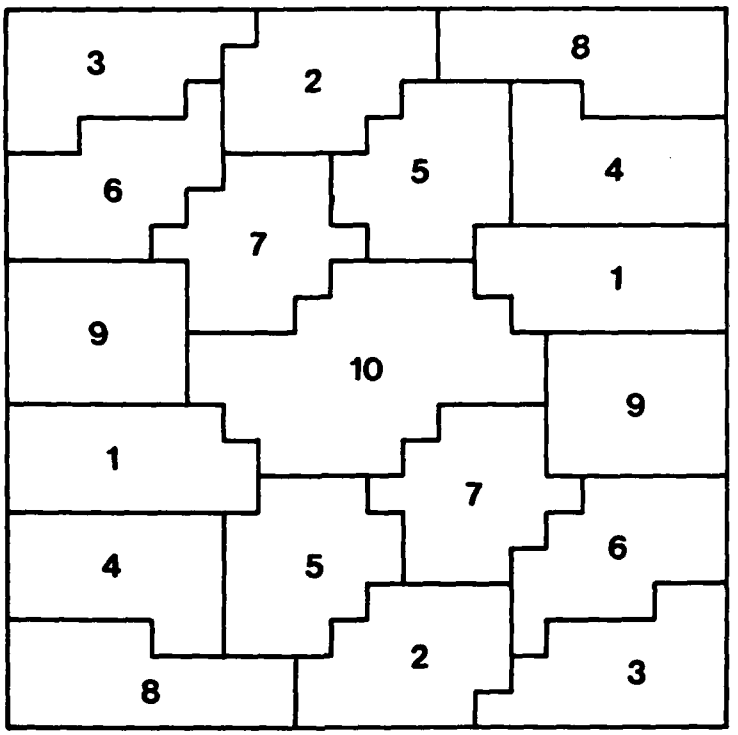

Figure 3-14. PCGH Designed for Uniform Illumination and 10 Equal Intensity Outputs. Facets are arranged symmetrically to provide immunity to beam wander.

numbers in each facet indicate the channel assignments. Spatial frequencies of the linear gratings are dictated by the system geometry. First-order diffracted light from a facet of spatial frequency ν will be focused in the detector plane a distance $\nu\lambda$ F from the transform lens axis (Figure 3-13), where λ is the wavelength and F the transform lens focal length. Our design is for a 10-element linear detector array. This requires 10 equally spaced grating frequencies. The widest possible detector separation is achieved with grating frequencies $(n + 9)\Delta\nu$, where $\Delta\nu$ is the frequency separation and $n = 1,2, \ldots,10$. Then the unwanted harmonic frequencies from the imperfect square-wave gratings begin at $20\Delta\nu$ and do not coincide with desired outputs.

Matrix values are encoded into the PCGH via grating area modulation. The hologram must therefore be divided into facets in such a way that the amount of light diffracted by a facet to its detector is proportional to the required matrix element. Various considerations lead us to partition the PCGH into facets along a rectangular grid.

Mathematically, the transmittance of a facet can be regarded as the product of its aperture and an infinite linear grating. By the Fourier convolution theorem, the diffraction pattern of this facet is the diffraction pattern of its aperture convolved with

the delta function from its grating. In other words, the effect of the linear grating is to shift the location of the diffraction pattern produced by the facet aperture.

Figure 3-15 indicates the diffraction pattern due to a square aperture of dimension D. The main lobe has a width of $2\lambda F/D$ and contains 81.5 percent of the energy passing through the aperture. The sidelobes form a rectangular array with sidelobe energy diminishing inversely as the square of the distance from either axis as indicated by Figure 3-16. Crosstalk therefore diminishes most rapidly for detectors spaced along a line oriented at 45 degrees to the facet boundaries. This requires the grating fringes to run diagonally within each facet.

As indicated earlier, the separation of detectors is $\Delta\nu\lambda F$. As facets are made smaller, their diffraction patterns become larger, producing undesirable crosstalk. For this reason, we impose a minimum square facet size D to produce a main diffraction lobe whose (diagonal) dimension $(2\sqrt{2})\lambda F/D$ is 2/3 the (diagonal) detector separation $\Delta\nu\lambda F$. In other words, the minimum facet size is $D = (3\sqrt{2})/\Delta\nu$. We size our detector aperture to capture only the main lobe of this minimum facet diffraction pattern for a calculated worst case crosstalk of 37 dB. A larger aperture would capture lesser lobes of the channel of interest, but also some greater lobes of adjacent channels, thereby degrading the channel separation. Also, having zero intensity at the edges of the detector aperture serves to ease aperture alignment tolerances.

The above discussion, of course, considers crosstalk when each facet is a minimum square facet. This would be a severe constraint on system numerical range. In practice, we form the facet for each channel from many of these minimum-sized modular subfacets. Therefore, the diffraction pattern for each channel is the coherent sum of all subfacets for that channel. Crosstalk can be minimized by clustering each channel's subfacets into one or two large facets, as was done in the PCGH of Figure 3-14. By requiring that large facets be built up of modular subfacets, we ensure that, no matter how complicated the diffraction pattern within a detector aperture, the intensity will still fall to zero at the aperture edges. Also, since subfacet boundaries are diagonal to the grating fringes, any bright sidelobes will occur diagonally away from adjacent detectors. This phenomenon is easily seen in Figure 3-20.

Partitioning the PCGH

Partitioning is the task of assigning subfacets to each channel in such a way as to achieve the correct relative intensities. This task is greatly simplified by our decision to adopt modular subfacets. The energy incident on a rectangular facet is easily computed for either uniform or Gaussian illumination. Each subfacet is assigned entirely to one channel. We assume that each channel receives several subfacets which can be grouped into one or more larger facets. Most of the diffracted energy from one of these larger facets should fall within the detector aperture. Therefore, the contribution of each subfacet to the total detected energy is approximately the product of its incident illumination and its diffraction efficiency. We need only compute this energy for each subfacet and then decide which subfacets are to be assigned to which channels. The error introduced by this approximation varies from near zero (many subfacets/facet) to 18.5 percent (one subfacet/facet).

E47069

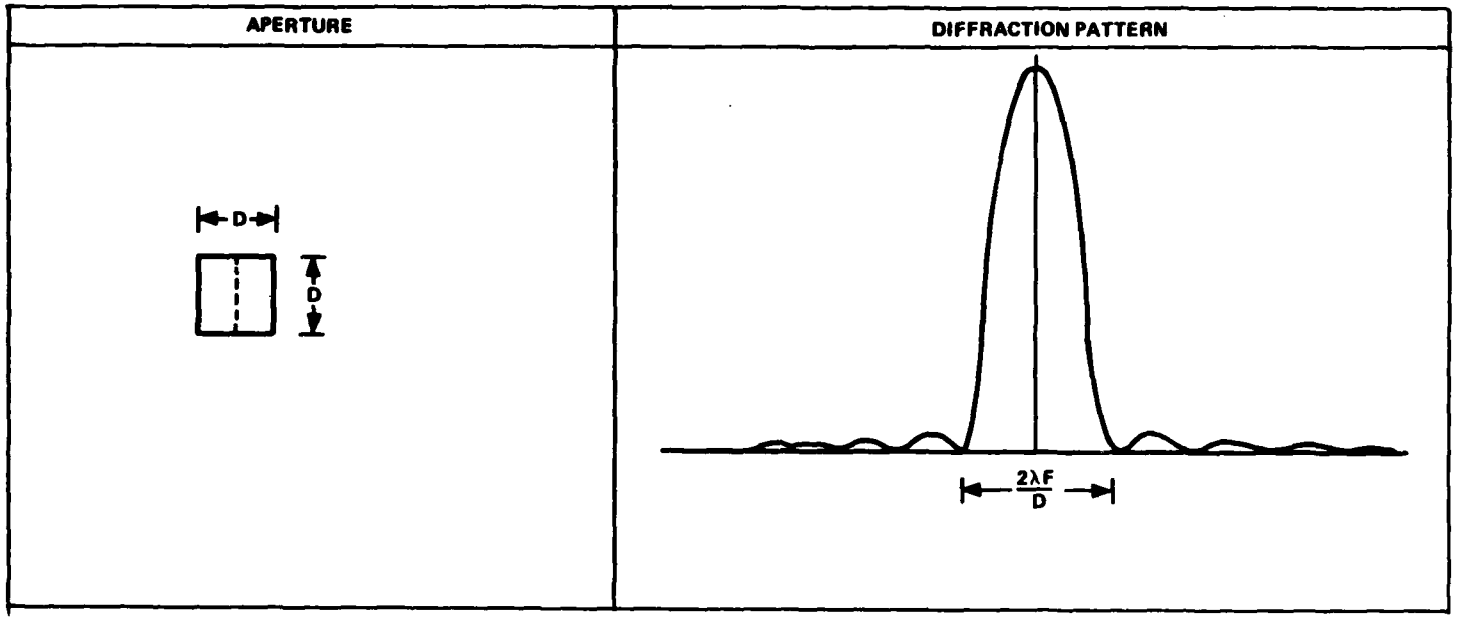

Figure 3-15. Square Aperture Diffraction Pattern. The central lobe contains 81.5 percent of the energy.

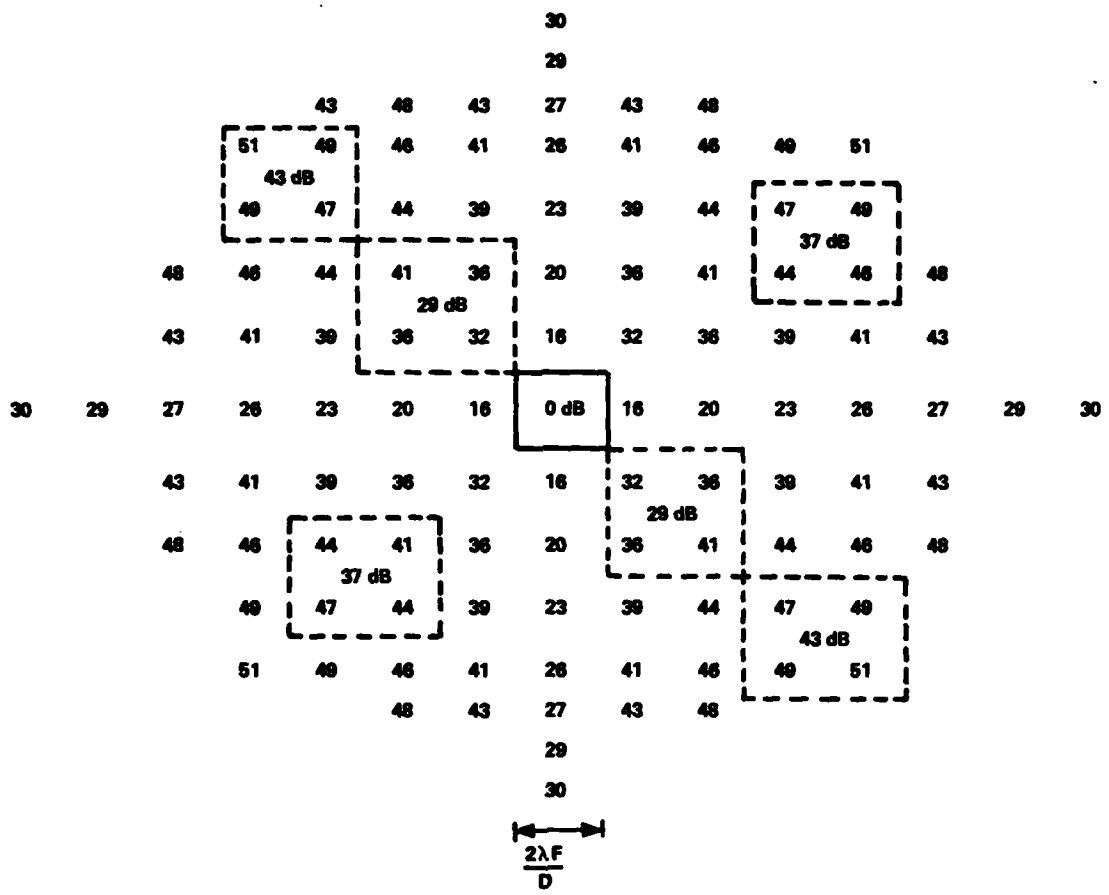

Figure 3-16. Relative Intensity of Sidelobes (dB) for Square Aperture Diffraction. A square detector captures the main lobe. Adjacent identical detectors (dashed boxes) must be separated diagonally to avoid bright on-axis sidelobes. Crosstalk (dB) is indicated for three alternative adjacent detector locations.

To have the greatest flexibility in partitioning the PCGH, and to minimize the approximation error, we would like the modular subfacets to be as small and numerous as possible. Since they are of size $D = (3\sqrt{2})/\Delta\nu$, we want a large spatial frequency separation $\Delta\nu$. However, a large spatial frequency separation implies large spatial frequencies and hence small grating periods. If the grating period becomes comparable to the e-beam spot size, considerable grating duty cycle errors, with corresponding diffraction efficiency errors, will result. For these reasons we have elected to use grating frequencies of 60 to 114 lp/mm (measured along either axis) and 0.5 mm subfacets. This gives us 400 subfacets in a 1 cm × 1 cm PCGH for a maximum numerical accuracy of about 20 dB. With Gaussian illumination, the effective number of subfacets is more than 5000, since the corner facets will have about 6 percent the intensity of illumination of the central facets, assuming a 1 cm ($1/e^2$) beam diameter.

A well partitioned PCGH can be characterized by the following four criteria:

- Subfacets for each channel should add up to the correct total power.
- Subfacets for each channel should form a single, compact facet.
- In the case of Gaussian illumination, facets for the dimmer channels should be located near the edges so that they may be made larger.
- In the case of Gaussian illumination, subfacets for each channel should be located symmetrically about the center to provide some immunity to beam wander.

It is generally not possible to simultaneously satisfy each of these criteria. For example, a facet cannot be symmetric about the center, located near the edge, and also compact. Some compromise is necessary.

The partitioning algorithm which we have developed uses a merit function to decide if a particular change to the PCGH is advantageous. The merit function, which embodies our four criteria, is

$$\begin{aligned} MF = {} & C_1 \times \Sigma\,|\text{relative intensity error}| \\ & + C_2 \times [\text{number of facet corners} + 2 \times \text{facet perimeter}] \\ & + C_3 \times \Sigma\,|\text{deviation from mean of facet size}| \\ & + C_4 \times [\text{number of asymmetrically assigned subfacets}] \end{aligned}$$

where the summations are over the various channels. The units of facet perimeter and facet size are D and D^2 respectively. The constants C_1, C_2, C_3 and C_4 are adjusted to give desired emphasis to the four criteria. This merit function is a negative trait in the sense that we wish to minimize it.

While the merit function provides a means of distinguishing the better of two partitionings of a PCGH, it does not tell us which partitionings to consider. With 400 subfacets and 10 channels, there are 10^{400} possible partitionings! An exhaustive search is out of the question. We have developed two algorithms for partitioning. One algorithm takes a starting PCGH (which may be blank) and considers all changes involving only one subfacet. Changes which would divide existing facets are rejected. Any other change which reduces the merit function is implemented. Although this algorithm can be somewhat restrictive, it has tended to work reasonably well. A second algorithm, which we have also found useful, allows two subfacets to swap their channel assignments. As is the case with most optical design codes, the operator must guide the partitioning to some extent, redefining the merit function according to how the PCGH is developing and choosing which algorithm to apply.

Figure 3-17 shows the partitioning algorithm at work on a PCGH having 20 × 20 or 400 subfacets. The goal was a hologram that would produce 10 equal intensity outputs when uniformly illuminated (40 subfacets/channel). Facet boundaries are indicated following the first, one intermediate and the last iteration. Figure 3-17c should be compared to the PCGH of Figure 3-14 which included a symmetry criterion in its merit function.

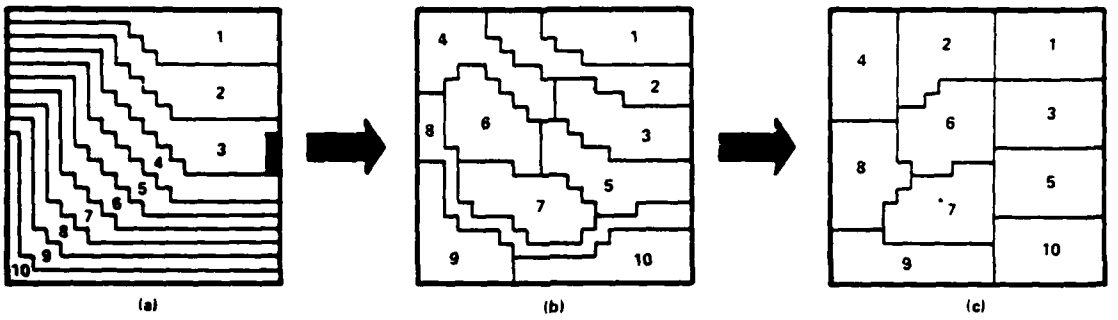

a) After the first iteration, facets branch from their starting points along the upper left margin.

b) Several iterations later, most facets are considerably more compact.

c) Final solution. The algorithm could find no further improvements.

Figure 3-17. Partitioning of a PCGH for Uniform Illumination and 10 Equal Intensity Outputs

Trimming Methods

To extend our numerical accuracy beyond about 20 dB, it is necessary to employ a separate lithography step to adjust the relative amplitudes of the outputs. The ability to do this trimming is one of the chief advantages of e-beam lithography and the PCGH. There are several possible methods of trimming a PCGH once it has been made and tested. The best trimming method is to add a negative facet, that is to say, a facet exactly out of phase with the existing facet. This is easier than it might sound: the negative facet can be written in space already occupied by the existing positive facet, leaving a completely open area in a portion of the positive facet. Linewidth problems are overcome and registration requirements reduced since, if we write over the whole area to be trimmed (i.e., not just when there is chrome), then the phase and duty cycle of the negative facet exactly complement the existing positive facet.

Experimental Results

The experimental setup for demonstration and evaluation of PCGHs is shown in Figure 3-18. The setup resembles Figure 3-13 except for the detector array, which has been replaced by a single, movable detector. Light from a He-Ne laser is spatially filtered to create a Gaussian point source which is then imaged in the detector plane by the lenses. The PCGH is kinematically mounted [3-11] on a micropositioner which affords three degrees of translation and one of rotation. Kinematic mounting allows removal for trimming and subsequent replacement of the PCGH without disturbing the alignment. In the detector plane, the single UDT-455 photodetector is

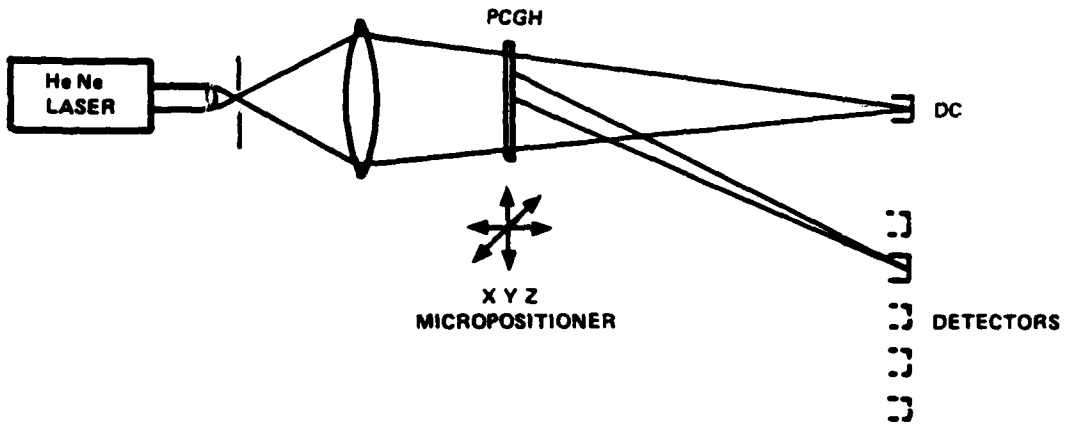

Figure 3-18. Experimental Setup for Demonstration and Evaluation of PCGHs. A single detector scans across the multiple output locations while a second detector monitors the undiffracted beam. Later experiments substitute a single-mode optical fiber for the spatial filter.

mounted on a motorized translation stage. The full width of the main lobe from a minimum-size facet in our system is 2 mm. One of several square apertures, selectable in size from 1 to 2 mm, is placed in front of the detector to define and limit its effective area. A second, identical photodiode monitors the DC beam to compensate for laser power fluctuations.

Alignment of the PCGH is straightforward. With the DC detector removed, the movable detector is positioned to receive maximum signal from the DC beam. The stage is then translated, and the PCGH rotated to maximize one of the other outputs. This aligns the outputs with the path of the detector and this alignment is unaffected by subsequent translation of the PCGH. Centering the PCGH on the optic axis is achieved by equalizing the signals from four open apertures located just outside the hologram boundaries. Translation of the hologram along the optic axis effectively determines beam diameter, since the beam is slightly converging in this region. Beam diameter is adjusted to yield best agreement with the design parameters.

The setup as described above was used to evaluate the PCGHs of Figures 3-14 and 3-17. These holograms were each designed to produce 10 equal intensity outputs when uniformly illuminated. Experimentally, the outputs differed by as much as a factor of two in intensity. Much of this variation was attributable to non-uniform illumination (an insufficiently expanded Gaussian). We therefore proceeded to experiments that would utilize the full Gaussian beam. Out of several PCGHs designed for Gaussian illumination, two were ultimately fabricated.

Figure 3-19 shows the partitioning by subfacets of a PCGH designed for Gaussian illumination and 10 equal outputs. Experimentally, we found the outputs to be equal to within 20 dB (Figures 3-20 and 3-21), a result we consider quite good for an optical

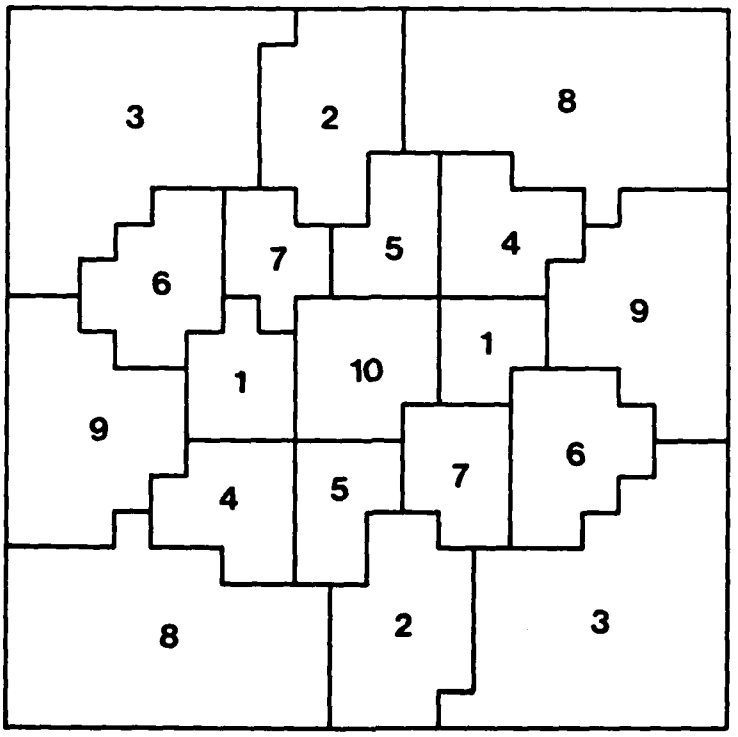

Figure 3-19. PCGH Designed for Gaussain Illumination (diminishing to $1/e^4$ at the corners) and 10 Equal Intensity Outputs. Symmetry provides some immunity to beam wander.

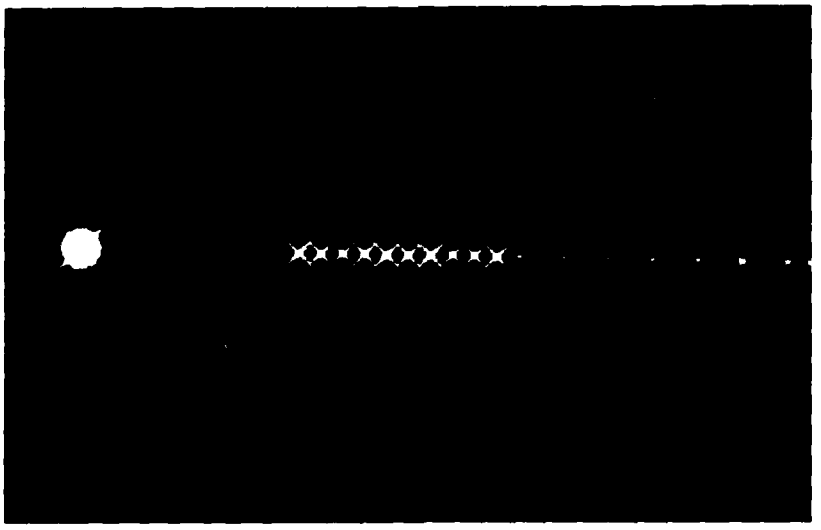

Figure 3-20. Diffraction Pattern for PCGH of Figure 3-19. The undiffracted beam, all 10 first-order beams, and several second-order beams are visible. Note that bright sidelobes occur away from adjacent channels.

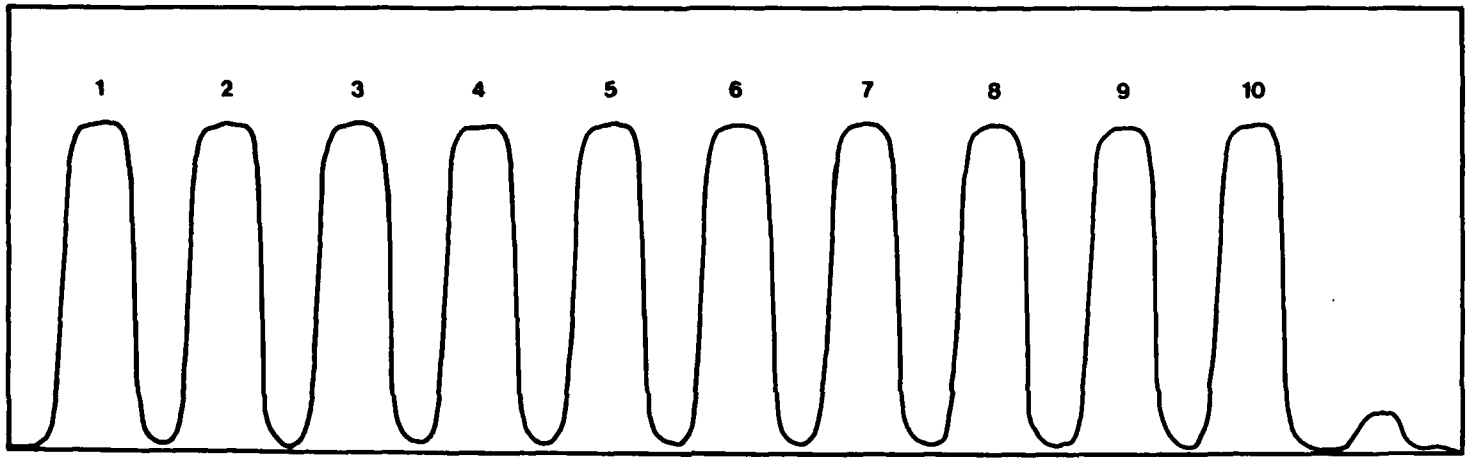

Figure 3-21. Scan Through Diffraction Pattern of Figure 3-20. The scan is through the centers of the outputs. The 10 peaks are equal in intensity to better than 20 dB.

computing scheme. A discouraging fact was that day-to-day stability of the setup was not much better than the 20 dB. The dominant problem here was beam wander in the laser, which manifested itself as time dependent pointing of the Gaussian point source. With this variability, improving the PCGH through trimming proved impossible.

Our objective of pushing the numerical accuracy beyond 20 dB demanded a more stable source of illumination. For this reason, we modified the experiment to use a single-mode optical fiber as the point source. A fiber offers distinct advantages over a pinhole spatial filter; the shape and pointing of the output beam are unrelated to what goes on at the input end. Unfortunately, the fiber output distribution was only approximately Gaussian. There were also difficulties in adequately stripping cladding modes and in increased sensitivity of intensity to input alignment.

When we evaluated the equal intensity output, Gaussian illumination PCGH of Figure 3-19 using the fiber optic source, the accuracy dropped from 20 dB to about 7 dB due to the different illumination profile. The PCGH of Figure 3-22, designed for Gaussian illumination and nine non-zero outputs spanning a 40 dB numerical range, had a measured numerical range with the fiber optic source of slightly under 37 dB. This 3 dB discrepancy was due to the two dimmest channels each occupying a full subfacet. Numerical accuracies of the other eight channels were about 7 dB. Although final accuracies were less than what we initially had hoped for, further refinement of this method could lead to a vector-matrix multiplication scheme with high accuracy, large numerical range, and high optical efficiency, particularly if implemented via phase gratings.

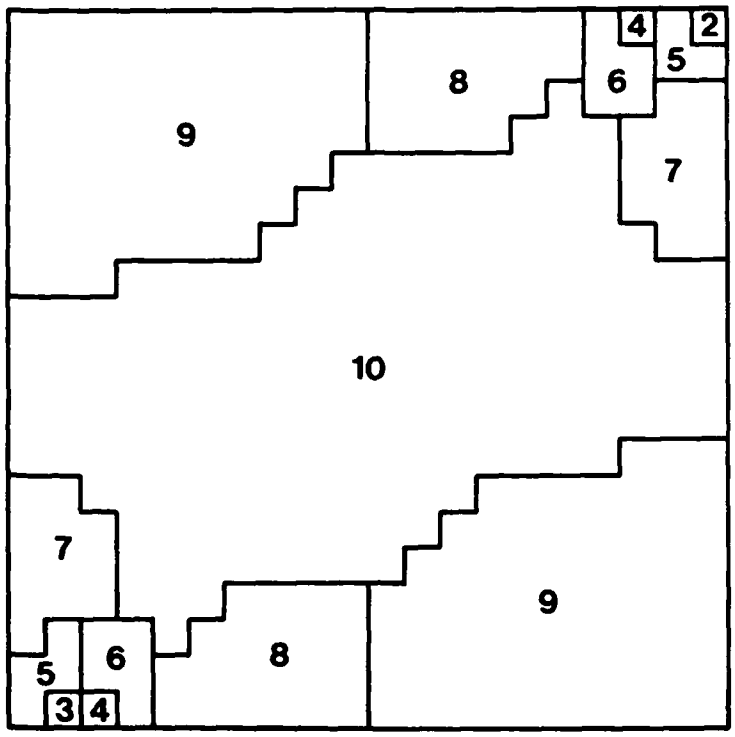

Figure 3-22. PCGH Design for Gaussian Illumination and 9 Non-Zero Outputs Spanning a 40 dB Numerical Range ($y_l = 0$, $y_m = 10^{m/2}$). Channel 10 occupies most of the bright central portion, whereas the dimmest channel is located in the corner where intensity is diminished by $1/e^4$.

REFERENCES

3-1 J.C. Wyant, and V.P. Bennett, "Using Computer Generated Holograms to Test Aspheric Wavefronts," Appl. Opt. *11*, 2833-2839 (1972).

3-2 J.S. Loomis, "Computer-Generated Holography and Optical Testing," Proc. Soc. Photo-Opt. Instrumen. Eng. *215* (1980).

3-3 A.J. MacGovern and J.C. Wyant, "Computer Generated Holograms for Testing Optical Elements," Appl. Opt. *10*, 619-624 (1971).

3-4 P.M. Emmel, and K.M. Leung, "A New Instrument for Routine Testing of General Aspherics," Proc. Soc. Photo-Opt. Instrumen. Eng. *171* (1979).

3-5 K.M. Leung, J.C. Lindquist, and L.T. Shepherd, "E-beam Computer Generated Holograms for Aspheric Testing," Proc. Soc. Photo-Opt. Instrumen. Eng. *215*, 70-75 (1980).

3-6 J.W. Goodman, A.R. Dias and L.M. Woody, "Fully Parallel, High-Speed Incoherent Optical Method for Performing Discrete Fourier Transforms," Opt. Lett. *2*, 1-3 (1978).

3-7 J.W. Goodman, A.R. Dias, L.M. Woody and J. Erikson, "Application of Optical Communication Technology to Optical Information Processing," Proc. Soc. Photo-Opt. Instrumen. Eng. *190*, 485-496 (1979).

3-8 K. Bromley, A.C.H. Louie, R.D. Martin, J.J. Symanski, T.E. Keenan and M.A. Monahan, "Electro-Optical Signal Processing Module," Proc. Soc. Photo-Opt. Instrumen. Eng. *180*, 107-113 (1979).

3-9 R.P. Bocker, "Matrix Multiplication Using Incoherent Optical Techniques," Appl. Opt. *13*, 1670-1676 (1974).

3-10 S.K. Case and P.R. Haugen, "Partitioned Holographic Optical Elements," Opt. Eng. *21*, 352-353 (1982).

3-11 W.J. Smith, *Modern Optical Engineering*, pp. 427-431, (McGraw-Hill, New York, 1966).

Section 4
Fabrication Techniques for Increased Diffraction Efficiency

Because of their low weight, small size and potentially easy replicability, diffractive optical elements are an attractive alternative to conventional optical elements in systems employing monochromatic light. In the two preceding sections, we have shown that e-beam computer generated holograms can have very large space-bandwidth products and produce arbitrarily prescribed wavefronts. The holograms we generated for optical testing and optical computing were binary, absorption type (chrome-on-glass) holograms with diffraction efficiencies limited to a theoretical maximum of 10.1 percent. In this section, we consider e-beam fabrication techniques for producing computer generated holograms offering much higher diffraction efficiency.

To exhibit high diffraction efficiency a hologram must utilize phase modulation rather than absorption modulation. Phase modulated holograms are typically characterized as either thick or thin, although the transition is a continuous one and intermediate types are common [4-1]. Thin phase holograms can be treated as two-dimensional phase-retardation plates, while thick phase holograms are three-dimensional recordings of interference patterns.

Thick phase holograms depend on periodic coupling along the propagation direction such that proper phase matching is achieved for only one diffracted order. When the refractive index modulation and film thickness are properly chosen, nearly all energy is coupled to this one order. Thick phase holograms, when interferometrically recorded in dichromated gelatin, can exhibit diffraction efficiencies approaching 100 percent [4-2]. Unfortunately, interferometric recording lacks flexibility for producing arbitrary wavefronts. It is also difficult to construct thick phase holograms for use at long wavelengths since efficient recording materials are not red or infrared sensitive.

One of our objectives has been to develop fabrication techniques for producing high diffraction efficiency e-beam computer generated holograms. We have restricted our consideration to holograms of the surface-relief type; while e-beam direct writing of phase gratings in amorphous chalcogenite films has been demonstrated, the index modulation ($\Delta n/n \sim 0.01$) and film thickness (<5 micron) are insufficient to permit diffraction efficiencies greater than a few percent. We have investigated two types of surface-relief holograms. The first type is a transmission hologram produced by ion milling of a dielectric substrate. The second type is a blazed, reflection hologram produced by anisotropic etching of a silicon substrate. The remainder of this section reports details of this work.

ION-MILLED HOLOGRAPHIC OPTICS

With slight modification, our e-beam fabrication procedure for chrome-on-glass absorption type holograms can also produce thin phase holograms in e-beam resist. The modification involves placing the metallization (required for conductivity during exposure) on top of the e-beam resist and then removing it by etching before resist development. The result is a square-wave grating in e-beam resist. Recently, it has been demonstrated that this technique is also capable of producing high-efficiency (60 to 70 percent) sawtooth grating profiles if the electron dose is suitably varied [4-4]. A disadvantage is that the resulting holograms are hygroscopic and lack environmental durability.

Rather than use the e-beam resist directly as a hologram, we use it as a mask for ion milling the grating pattern into the glass (or quartz) substrate. This produces an all-glass hologram that is very environmentally durable. It is also nonabsorptive, making it capable of high diffraction efficiency and a high damage threshold. The following paragraphs discuss these ion-milled holograms in detail.

Theory

Dielectric surface-relief gratings have received extensive theoretical treatment [4-5]. At low spatial frequencies (grating period $>>$ 1 wavelength) these holograms behave as thin phase gratings. They typically produce many diffracted orders (Figure 4-1) whose intensities depend on the groove profile. A square-wave profile, as produced by ion milling, yields a maximum diffraction efficiency of 40.5 percent. This maximum occurs for a milling depth corresponding to a phase retardation of π radians and a groove width equal to half the grating period.

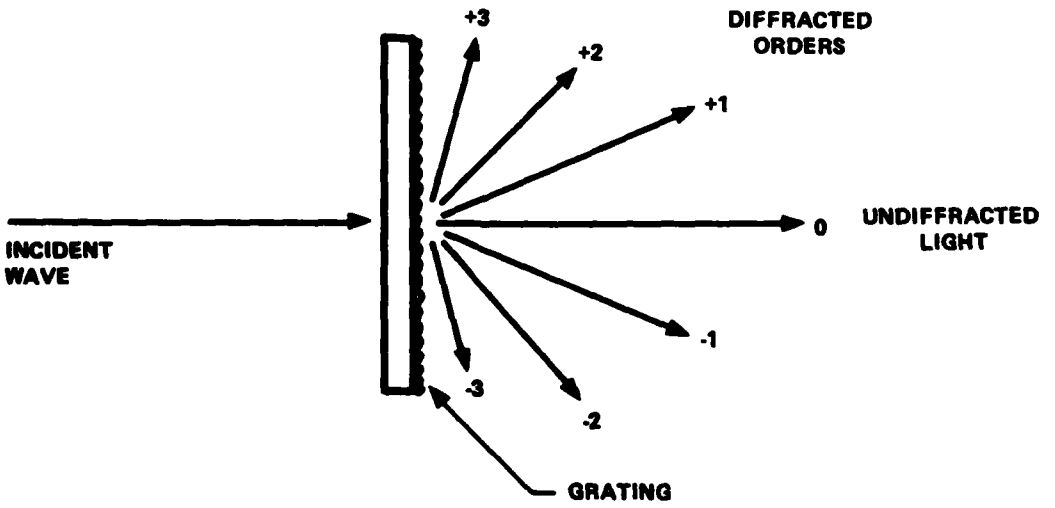

Figure 4-1. Diffraction by a Low Spatial Frequency Ion-Milled Grating. Many diffracted orders compete for incident light, with no single order receiving more than 40.5 percent of the total. Diffraction efficiency depends only weakly on angle of incidence.

We have developed a numerical model for analyzing square-wave, surface-relief gratings, adopting the rigorous, modal solution of Kaspar [4-6] and Burckhardt [4-7]. Some results of this modeling are shown in Figures 4-2 and 4-3.

Figure 4-2 shows the dependence of diffraction efficiency on milling depth for a 10-micron period grating. We have assumed a groove width-to-spacing ratio of 0.5, a wavelength of 6328Å, and normal incidence. Reflection losses at the grating surface have been included, but those at the opposite surface of the substrate have not, since this surface could presumably be antireflection coated. It is seen that variations in milling depth of ±10 percent can be tolerated before diffraction efficiency is reduced appreciably. Extinction of the undiffracted (zero-order) beam provides a sensitive indicator of optimum milling depth.

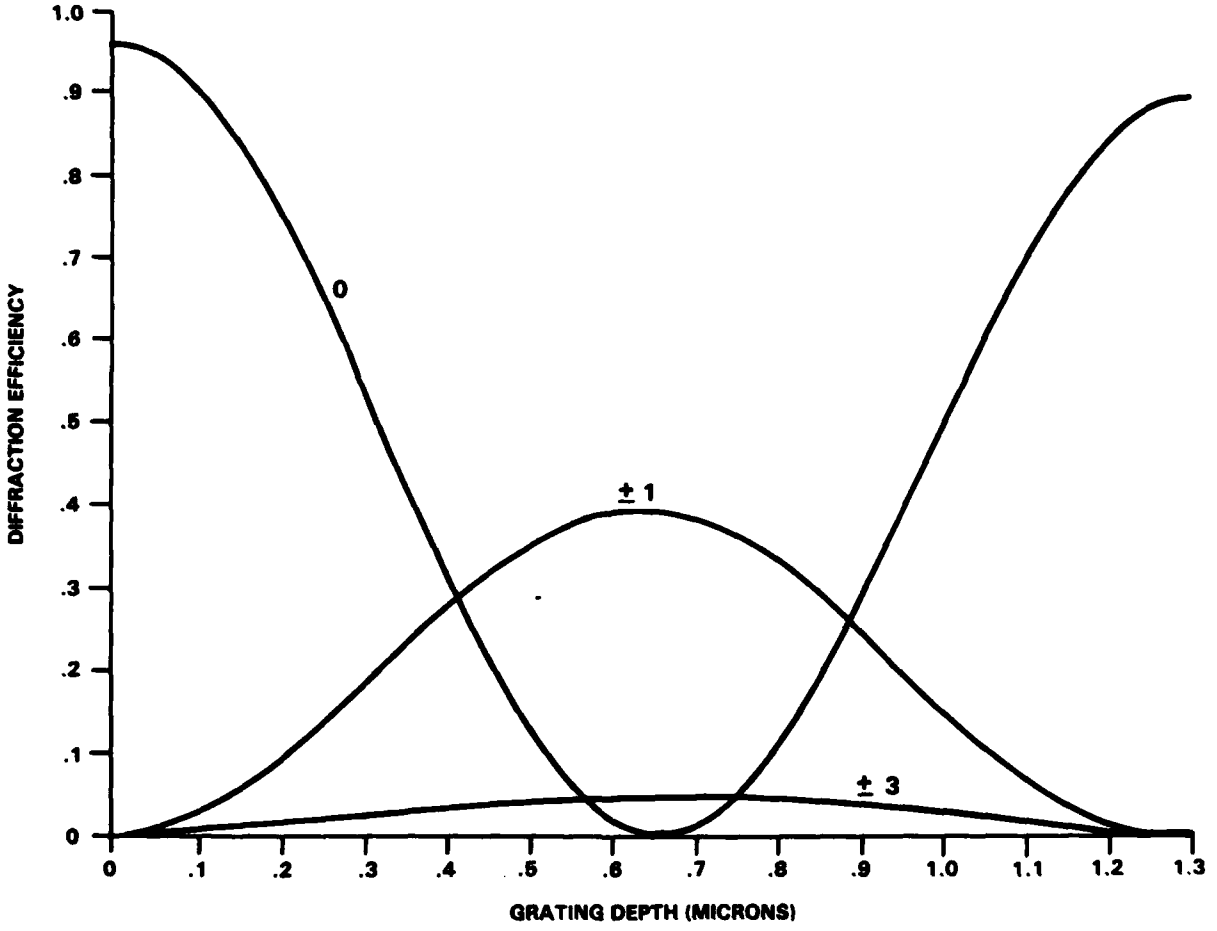

Figure 4-2. Diffraction Efficiency Versus Groove Depth for Ion-Milled Holographic Optics. A refractive index of 1.5 and normal incidence have been assumed. Maximum diffraction efficiency occurs for a milling depth of one wavelength, corresponding to a phase depth of π radians.

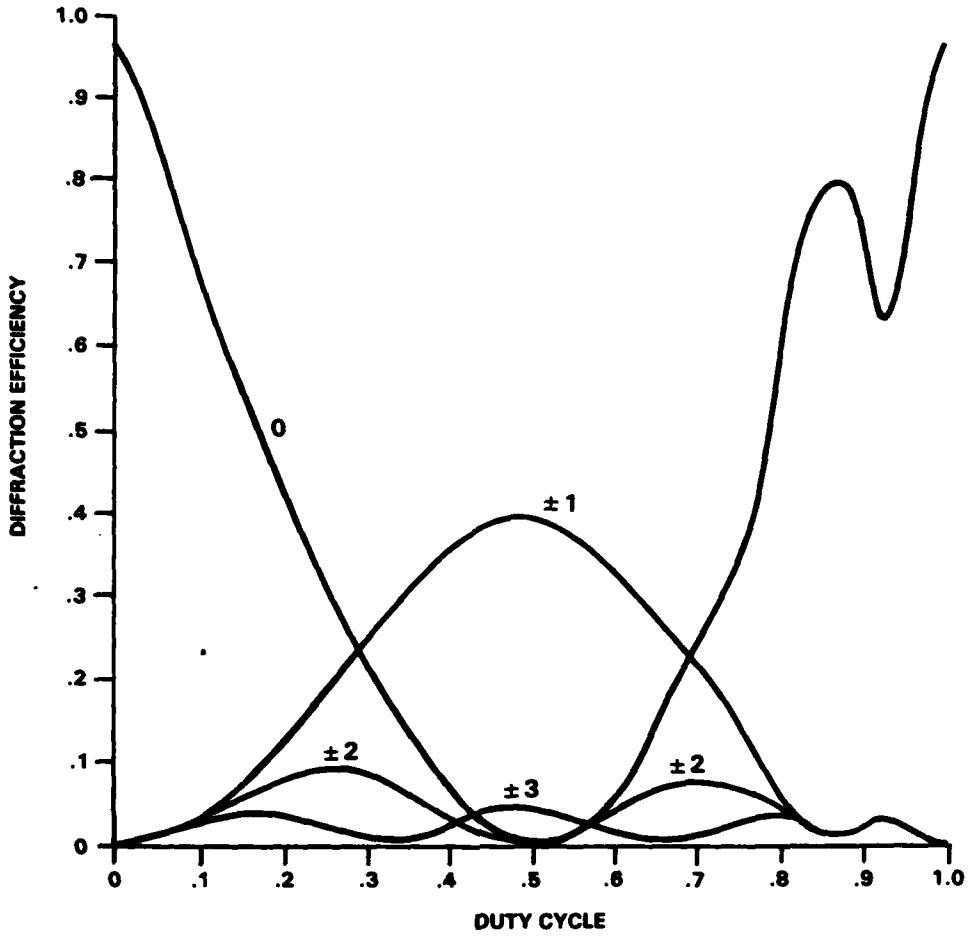

Figure 4-3. Diffraction Efficiency Versus Groove Width for Ion-Milled Holographic Optics. Maximum first-order diffraction efficiency occurs for a groove width-to-spacing ratio of 0.5. Optimum groove width is verified by the absence of even diffracted orders.

Figure 4-3 shows the dependence of diffraction efficiency on groove width for the same grating parameters as Figure 4-2. The milling depth has been optimized for maximum diffraction efficiency. It is seen that groove width must be controlled to a fraction ($\sim 1/10$) of the grating period in order to maximize first-order diffraction efficiency. Absence of the second diffracted order provides a sensitive indicator of optimum groove width. Figure 4-3 is invalid for either very large or very small groove widths since the sine series used to represent the square-wave groove profile was truncated at ten terms.

At low spatial frequencies, surface-relief gratings produce many diffracted orders as was shown in Figure 4-1. As grating period is decreased, fewer diffracted orders are available to compete for the incident light. Also, as the diffraction angles become

larger, the three-dimensional nature of the groove profile becomes important and these gratings can no longer be treated as simple phase-retardation plates. The polarization state of the incident beam also becomes significant.

We expect maximum attainable diffraction efficiency to increase with grating spatial frequency. At ultra-high spatial frequencies, the geometry is such that only one forward-diffracted order can exist to compete for incident light; all other orders being evanescent. This situation is depicted in Figure 4-4. The minimum spatial frequency to just satisfy this condition corresponds to a grating period of 1.5 wavelengths and an incident angle $\theta_0 = \sin^{-1}(1/3) = 19.5$ degrees. Unfortunately, our model suffers numerical inaccuracies when groove depth becomes comparable to groove spacing. We have therefore been unable to analyze holograms of ultra-high spatial frequency. However, there are a number of theoretical and experimental results to indicate that maximum diffraction efficiency increases with increasing spatial frequency. Moharam and Gaylord [4-5] have calculated a diffraction efficiency of 88.5 percent for a square-wave grating of period 1 wavelength and depth 1.55 wavelengths. Enger and Case [4-2] have demonstrated 88-percent diffraction efficiency for photoresist gratings of period 0.33 micron and depth 0.37 micron. We therefore expect an increase in diffraction efficiency as groove depth becomes comparable to groove spacing.

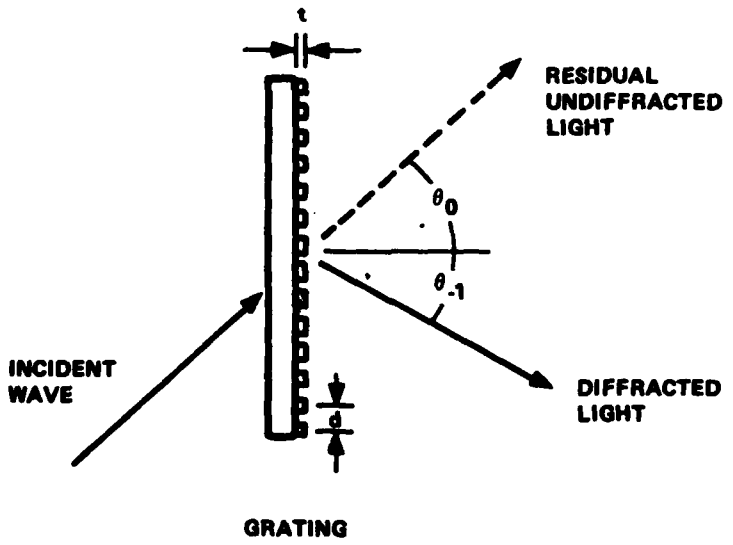

Figure 4-4. Diffraction by an Ultra-High Frequency Ion-Milled Grating. The geometry is such that only one diffracted order is transmitted; all others are evanescent.

Design

Figure 4-5 illustrates our basic design for an ion-milled holographic lens. We wished to demonstrate a high diffraction efficiency, large numerical aperture (NA) lens which would focus a collimated He-Ne laser beam to a diffraction limited point. The diffraction limited focal spot size is $\Delta x \geq \lambda/NA$, where $NA \approx \sin [\tan^{-1} (R/f)]$. Fabrication difficulty is related to the smallest grating period Λ_{min}. We fix the maximum grating period at $\Lambda_{max} = 2\ \Lambda_{min}$ in order to assure angular separation of the first diffracted order, limit the range of feature sizes to be drawn, and avoid possible lower diffraction efficiency at lower spatial frequencies. These considerations led us to the geometry depicted in Figure 4-5.

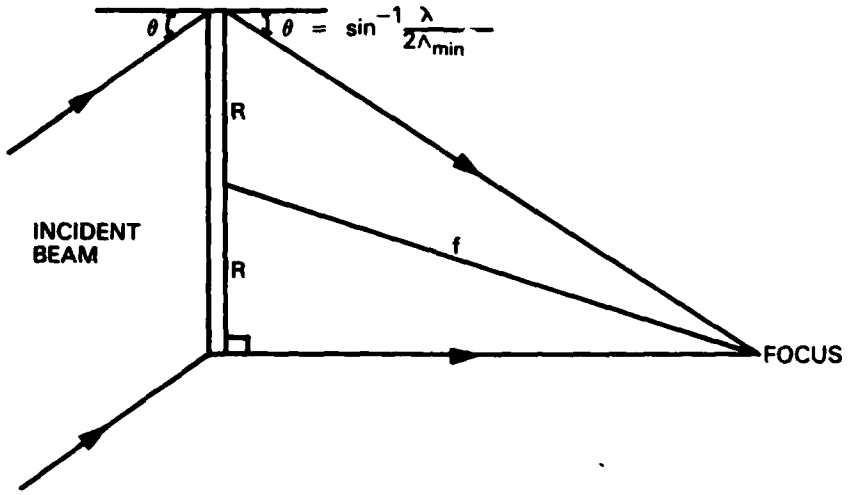

Figure 4-5. Design for Ion-Milled Holographic Lens. The lens focuses a collimated He-Ne laser beam to a point.

Table 4-1 lists the parameters of several holographic lenses we have designed along the lines of Figure 4-5. The quantity of data required to specify one of these lenses is related to both Λ_{min} and to hologram diameter. We arbitrarily selected a diameter of 5 mm for these lenses. In cases where the data quantities became excessive (all but CGH100 and CGH101), we specified cylindrical lenses with focal power in only one axis. Design CGH110C, requiring a 0.5-micron line width, taxed the resolution limit of our e-beam lithography system.

Fabrication Techniques

Figure 4-6 illustrates the basic fabrication process for ion-milled holographic lenses. The initial lithography is essentially the same as for our standard chrome-on-glass fabrication process depicted in Figure 1-3. A metallization layer is still required for electrical conductivity during exposure, so we generally use commercially available

Table 4-1. Ion-Milled Holographic Lens Designs

Identifier	Focal Length (mm)	f-number	Λ_{min} (microns)	Fringes
CGH100	160	f/32	10.2	370
CGH101	80	f/16	5.1	739
CGH102	40	f/8	2.5	1474
CGH103	30	f/6	1.9	1959
CGH108	25	f/5	1.6	2329
CGH109	20	f/4	1.3	2906
CGH110	15	f/3	1.0	3733

plates, which come with a layer of chrome (~650Å) and resist (6000Å PMMA) already deposited. After exposure and development, the resist acts as an etch mask for ion milling of the grating pattern into the glass substrate.

The relative milling rates of the various materials determine the depth to which we can mill into the substrate. Milling is done with argon ions in an Ion Tech dual beam ion mill. Relative milling rates of key materials are indicated in Table 4-2. Our standard glass-chrome-PMMA mask plates can only be milled to a depth of 2200Å before the PMMA is entirely depleted. From Figure 4-2, we see that a depth of about 6000Å is required for maximum diffraction efficiency. Chemical etching of the chrome from exposed regions would increase milling depth to only 2800Å before both PMMA and chrome were depleted. Instead, our procedure is to first etch through the chrome to create a chrome-on-glass hologram, but then use it as a mask for contact printing the hologram pattern onto a second glass plate coated with 7000-8000Å of photoresist. The lower ion etch rate of photoresist then allows milling to the required depth.

While the contact printing method works well for producing low spatial frequency holograms, it does not allow the full resolution capability of e-beam lithography to be utilized. We have, therefore, developed two alternative fabrication processes for holograms of high spatial frequency.

Our first alternative process replaces the PMMA with a Honeywell-proprietary e-beam resist, EP25H. This resist has half the ion etch rate and twice the sensitivity of PMMA. A 6500Å layer of EP25H allows milling to the optimum depth before both resist and chrome are depleted. With faster etching quartz substrates, the thickness of EP25H can be reduced to about 3000Å, allowing still higher resolution patterns to be drawn.

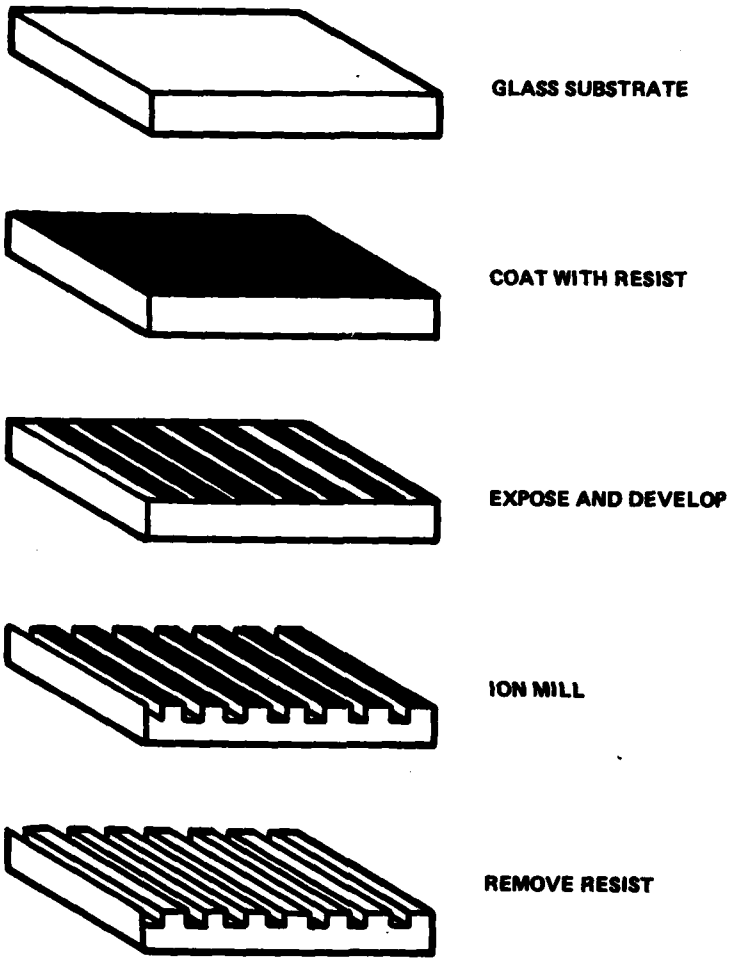

Figure 4-6. Fabrication Process for Ion-Milled, Holographic Optics. E-beam lithography is used to produce a hologram in resist on a glass substrate. The resist then serves as a mask for ion milling the hologram into the glass. After removal of the resist, we are left with a high-efficiency, all-glass hologram.

Table 4-2. Ion Beam Etch Rates (500 eV Argon Ions at 1 mA/cm^2, normal incidence)

Glass (soda-lime)	200 A°/min
Quartz	400
PMMA e-beam resist	550
EP25H e-beam resist	200
Chrome	530
AZ1350 photoresist	230

Our second alternative fabrication process, shown diagrammatically in Figure 4-7, is the ultimate in contact printing. A chrome-on-glass hologram is coated directly with photoresist and then exposed by illuminating from the back side. The chrome serves as an exposure mask, while the developed photoresist serves as an etch mask for ion milling. As long as the chrome remains intact, the process can be repeated as many times as necessary for milling to any desired depth. This process allows precise control of milling depth since the resist can be removed to check groove depth and then replaced for final milling to desired depth. With quartz substrates and UV exposure, this technique can be extended to very high resolution patterns.

Experimental Results

We have been quite successful in fabricating low spatial frequency holographic lenses with diffraction efficiencies near the theoretical limit of 40.5 percent. Achieving a groove width-to-spacing of 0.5 has proven to be a greater challenge than achieving the correct milling depth, particularly for higher spatial frequency patterns. This difficulty in controlling groove width prevented us from attaining the higher diffraction efficiencies we had hoped for at grating periods near 1 micron.

Figure 4-8 is an SEM photo of the ion-milled holographic lens CGH100. This f/32 lens has a near optimum square-wave groove profile, as can be seen by examining its diffraction pattern in Figure 4-9. The incident laser beam was somewhat larger in diameter than the hologram, causing the bright ring around the position of the undiffracted N = 0 order. The bright spot to the right of this ring is the focused N = +1 order beam, while the bright disk to the left is the N = 1 order beam for which the hologram acts as a negative lens. The fainter images to either side are the N = ±3 order beams. The darkness of the N = 0 order and the absence of any even (N = ± 2) orders attest to the optimum groove profile.

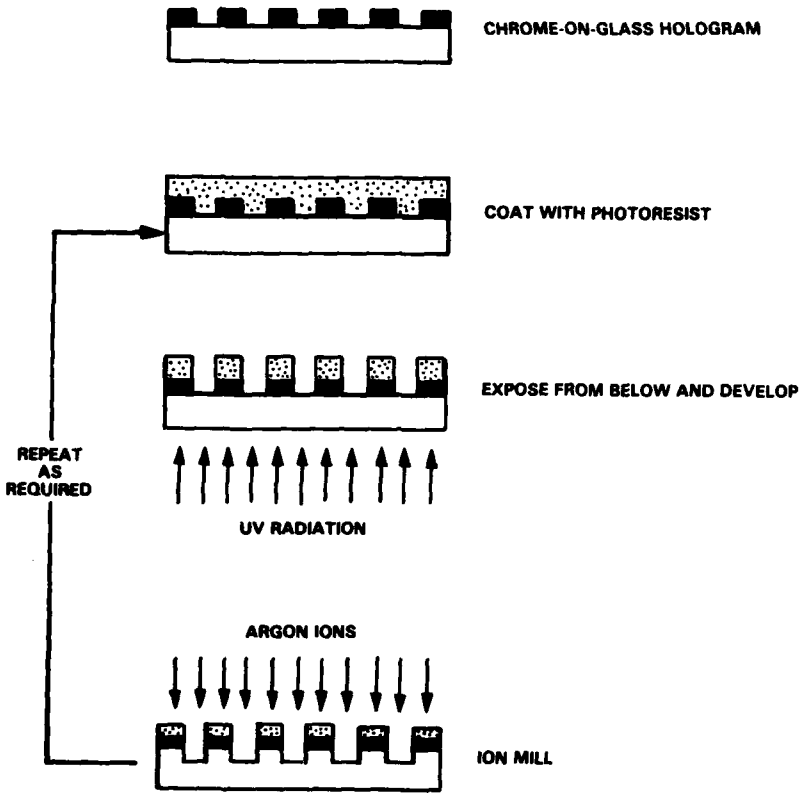

Figure 4-7. Alternative Fabrication Process for Ion-Milled Holographic Optics. This process allows deeper milling since the photoresist, which has a lower milling rate than e-beam resist, may be applied repeatedly.

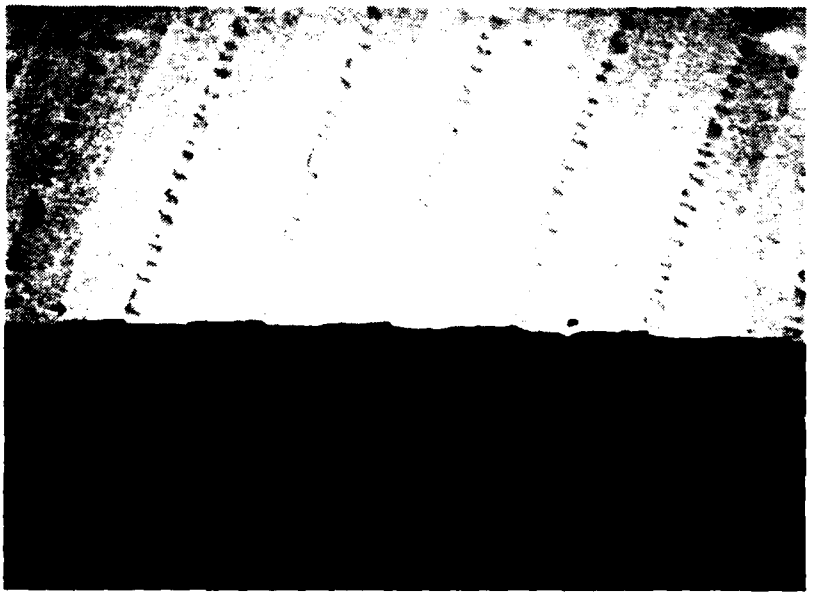

Figure 4-8. SEM Photo of Ion-Milled Holographic Lens CGH100. The groove spacing is about 10 microns.

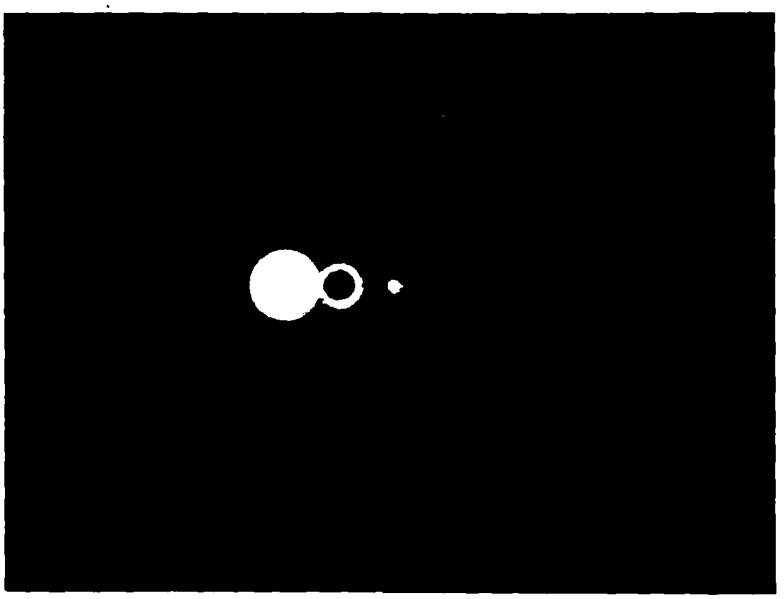

Figure 4-9. Diffraction Pattern from Ion-Milled Holographic Lens CGH100. The center of the ring is the N = 0 order, while the bright spot to the right is the focused N = +1 order.

Figure 4-10 is an SEM photo of the cylindrical holographic lens CGH110C. This lens, with a grating period of 1.0 micron, is the highest spatial frequency lens we have fabricated. Control of linewidth in the relatively thick (5000Å) resist during exposure and subsequent ion milling proved exceedingly difficult. The small feature sizes required that each sample be produced by e-beam direct-writing. This limited the number available for process development. Of several samples fabricated, none had a diffraction efficiency exceeding 20 percent.

To summarize, we found that we could fabricate ion-milled holographic lenses having diffraction efficiencies near the theoretical maximum of 40.5 percent if grating periods were greater than about 2.5 microns. Theory predicts an increase in diffraction efficiency for grating periods of 1 micron and under, but difficulties in controlling the grating profile at such small geometries resulted instead in reduced diffraction efficiency.

BLAZED, CRYSTALLINE HOLOGRAPHIC OPTICS

Our second approach to achieving high diffraction efficiency holographic optical elements uses anisotropic etching of crystals to produce blazed, reflection holograms. Blazed diffraction gratings are often made by ruling techniques and can have diffraction efficiencies approaching 100 percent. Anisotropic etching techniques are

Figure 4-10. SEM Photo of Ion-Milled Holographic Lens CGH110C. The groove spacing is about 1 micron.

used to create grating patterns for distributed feedback laser diodes [4-8]. Figure 4-11 shows one such grating. Our approach has been to combine e-beam lithography with anisotropic etching to produce blazed, holographic lenses in silicon substrates.

Theory and Fabrication Techniques

The anisotropic etching of silicon is a technique of growing importance for the fabrication of both integrated circuits [4-9] and micromechanical structures [4-10, 4-11]. Several ternary liquid etchants have been reported that etch silicon at different rates in the principle crystallographic directions. These consist of an oxidant such as potassium hydroxide (KOH), which oxidizes silicon to hydrated silica, and a complexing agent such as iso-2-propyl alcohol (IPA), which reacts with the silica to form a soluble complex ion [4-12]. Figure 4-12 indicates the principle crystallographic planes of (100) silicon. The (111) planes are the slowest etching planes. The (110) and (100) planes can etch 400 times faster than the (111) planes. Whether the (110) plane etches faster than the (100) plane, or vice versa, depends upon the etch formulation used. The fastest etching plane is the (211) plane. The etchant does not attack Si_3N_4 or SiO_2.

The fabrication process for blazed, crystalline grating structures is depicted in Figure 4-13. E-beam lithography is used to delineate a grating pattern in a Si_3N_4 or SiO_2 etch mask on (100) silicon. The grooves must be nominally parallel to the slow etching (111) planes. Etching proceeds in the (100) direction (down) and is stopped by

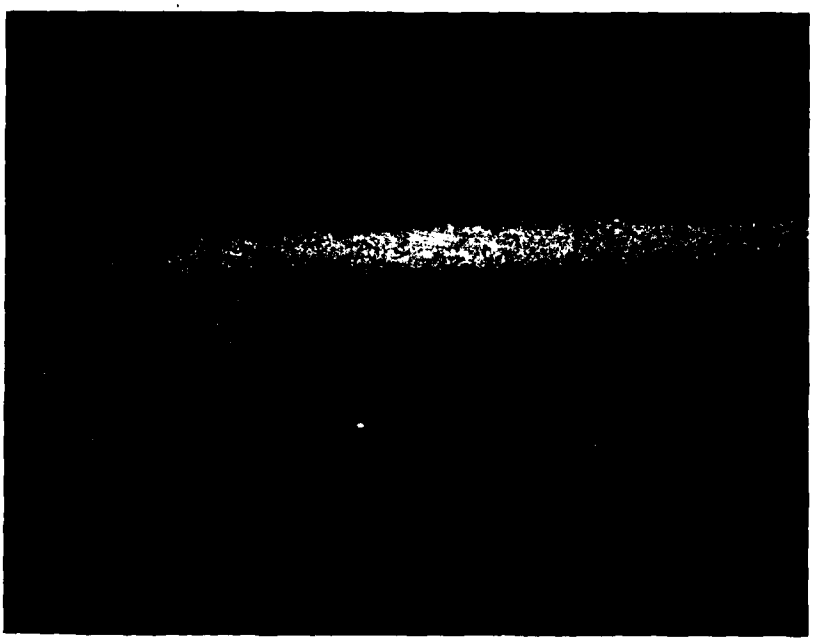

Figure 4-11. SEM Photo of Anisotropically Etched Grating in Gallium Arsenide. The cleaved edge view shows the vee-groove profile. This 0.376-micron linear grating was interferometrically recorded.

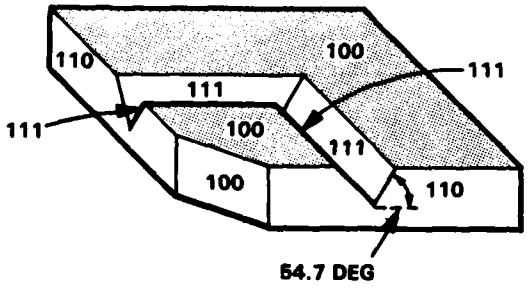

Figure 4-12. Orientation of Major Crystallographic Planes in (100) Silicon

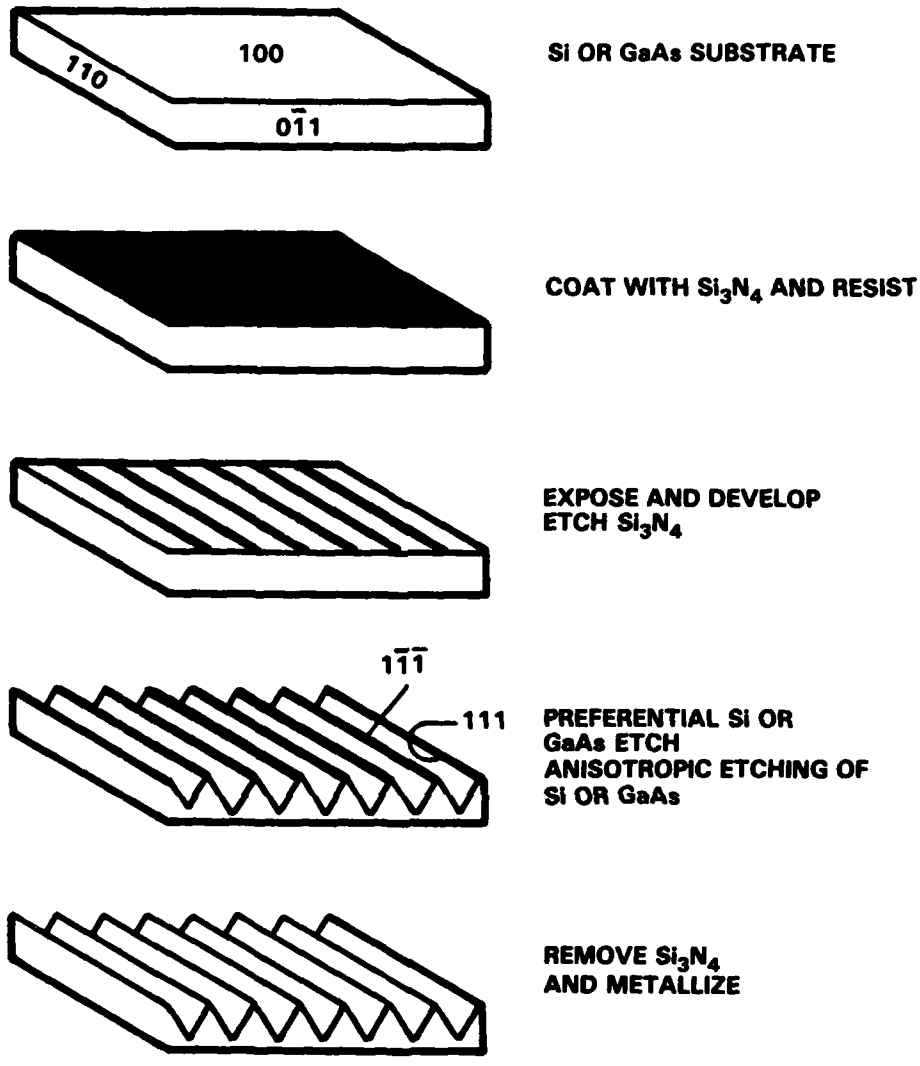

Figure 4-13. Fabrication Process for Blazed, Crystalline Holographic Optics. E-beam lithography is used to produce a hologram in Si_3N_4 on (100) silicon. The narrow lines of resist must run roughly parallel to the (111) planes. The anisotropic etch is stopped by the Si_3N_4 mask and the (111) planes, leaving precise vee-grooves. After cleaning, the hologram is metallized or used as a master for embossing copies.

the mask and the (111) planes, leaving precise vee-grooves with faces inclined at 54.7 degrees to the substrate normal.

Diffraction by a blazed, crystalline holographic grating is depicted in Figure 4-14. Diffraction angles are determined by the groove spacing and the grating equation. Tilted groove faces preferentially reflect light into particular diffracted orders. When both the grating equation and the reflection law can be satisfied simultaneously, much of the incident energy is channeled into a single diffracted order.

As blaze angles go, the 54.7-degree blaze produced by etching of (100) crystals is very steep. Other blaze angles are possible, but would require specially cut crystals. Very high blaze-angle gratings, because of their symmetric groove profiles, show peculiar first-order diffraction efficiencies [4-13]. Diffraction efficiency is found to depend significantly on polarization state and on departure from Littrow configuration (zero angular deviation).

The sharply peaked grating profile, as depicted in Figure 4-14, poses a number of fabrication difficulties. The linewidth of the etch mask pattern must, of course, be sufficient that undercutting does not free the mask before the vee-grooves are etched to their full depth. Any excess width will result in a flat-topped grating profile which reduces diffraction efficiency by preferentially directing light into the zero-order (undiffracted) beam. Flat tops become flat bottoms if the etched hologram is used as a master for embossing copies. Flat bottoms filling less than 1/3 of the groove depth will be shadowed by adjacent peaks.

Design

There are a number of design constraints associated with blazed, crystalline holographic optics. These can be attributed primarily to the fixed blaze angle and groove orientation imposed by the crystal geometry.

Figure 4-15 shows our designs for blazed, crystalline holographic lenses. The central ray is oriented so that it will be specularly reflected off the groove faces. In addition, we require that the incident angle be shallower than the diffraction angle. This prevents rays from striking the opposite face of a groove as they leave the grating and provides our rationale for distinguishing between collimators and condensers. To maximize numerical aperture, we make the collimated beam as large as possible without engulfing the point source or focus.

Blazed gratings can be designed to operate in nearly any diffractive order. Very high blaze-angle gratings are rarely used in first order [4-13]. The advantage of a higher order is that the grating period can be larger (although the required spatial accuracy is unaffected). A disadvantage is that adjacent orders are closer in angle and may compete for the light. This is a problem particularly for our blazed, crystalline holographic optics, since the grating period will vary but the blaze angle will not. Therefore, we might expect the largest numerical aperture when working in the first order. However, the small grating periods required ($\lambda/\sqrt{6}$ in Littrow configuration) make first-order blazed, crystalline gratings impractical.

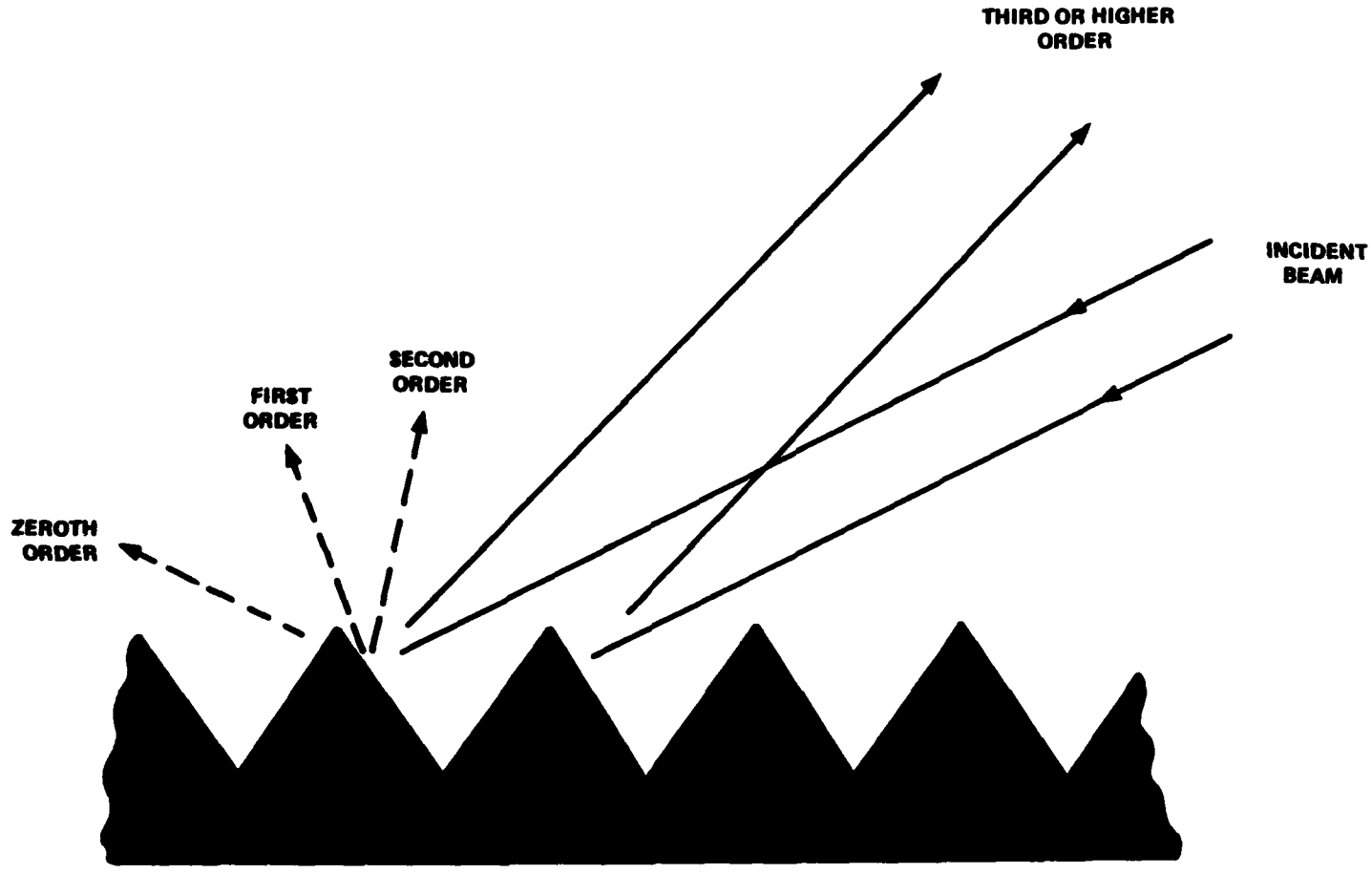

Figure 4-14. Diffraction by a Blazed, Crystalling Holographic Grating. Diffraction angles are determined by the groove spacing and grating equation. The tilted groove faces preferentially reflect light into a particular diffracted order.

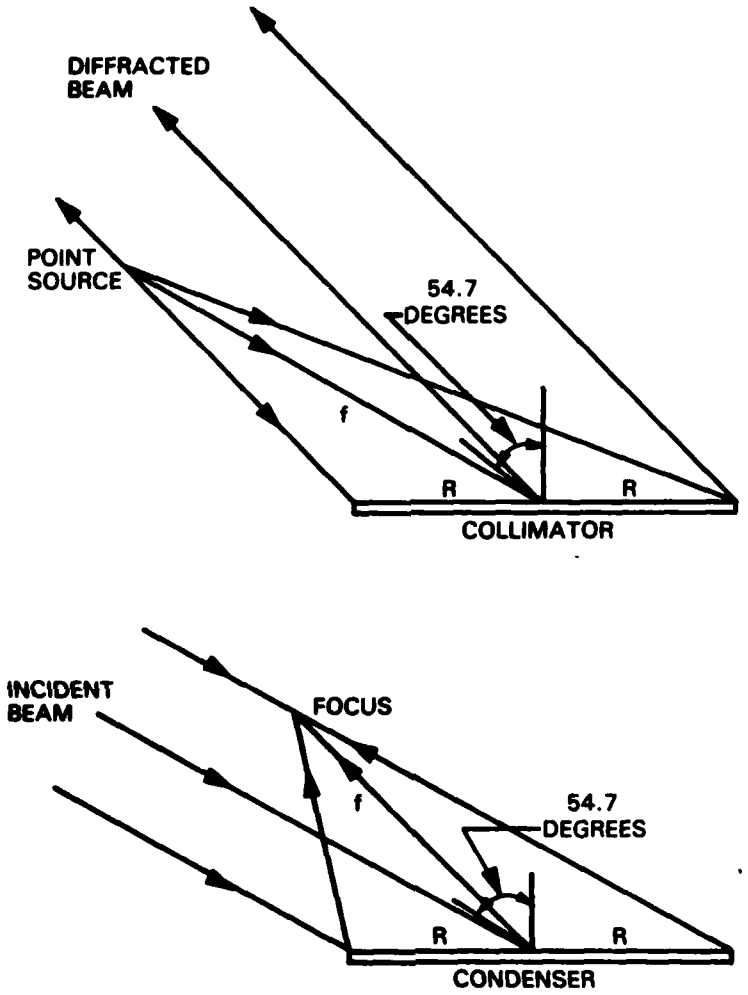

Figure 4-15. Two Designs for Blazed, Crystalline Holographic Optics. The geometry has been chosen so that the central ray will be specularly reflected off the groove faces, which are inclined at 54.7 degrees. In order that light not undergo multiple reflections, the incident angle must be steeper than the diffraction angle. This criterion fixed the point source (or focus) at the edge of the collimated beam.

Table 4-3 lists parameters of several blazed, crystalline holographic lens designs. These holograms are 5 mm in diameter and designed for operation at the He-Ne (6328Å) wavelength. In each case, the diffractive order was chosen as large as possible without having the blaze angle favor adjacent orders over some portion of the hologram. A line width-to-spacing ratio of 2/3 was chosen for these holographic lenses with the intention of replicating by embossing.

Table 4-3. Blazed, Crystalline Holographic Lens Designs

Identifier	Focal Length (mm)	f-number	Λ_{min} (micron)	Order	Type	Fringes
CGH104	80	f/16	2.7	7th	Condenser	1841
CGH105	80	f/16	2.7	7th	Collimator	1836
CGH106	40	f/8	1.5	4th	Condenser	3382
CGH107	40	f/8	1.5	4th	Collimator	3222

Experimental Results

Our attempts to fabricate blazed, crystalline holographic lenses were plagued by undercutting of the Si_3N_4. While some undercutting was expected, the magnitude of the effect was not well understood.

As an example, we describe the fabrication of the lens CGH104. This lens was designed as a 7th order f/16 condenser with a minimum grating period of 2.7 microns. The pattern was drawn as a chrome-on-glass mask with a line width-to-spacing ratio of 2/3. This hologram was then printed in AZ1450B photoresist on (100) silicon substrates coated with a 1500Å layer of Si_3N_4. Plasma etching was used to open grooves in the Si_3N_4.

The anisotropic etchant used for CGH104 consisted of 160 gm KOH in 110 ml IPA and 200 ml water. Figure 4-16 shows the sample after etching for 12 minutes at 35°C. In Figure 4-16a, undercutting of the Si_3N_4 mask is nearly complete, and yet the vee-grooves still do not have sharp bottoms. Also, the sides of the grooves show numerous ledges. Figure 4-16b shows another portion of the hologram where the mask has lifted off completely and some of the peaks have begun to erode. Still, the grooves do not have sharp bottoms.

Some undercutting of the mask and ledge formation on the (111) faces were expected due to misorientation of the grooves with respect to the true (111) planes [4-14]. For a perfectly oriented sample, with grooves parallel to the (111) planes, the rate of downward etching is $r_{(100)}$, while the rate of undercutting is $r_u = \sqrt{(3/2)}\, r_{(111)}$. Here $r_{(100)}$ and $r_{(111)}$ are etch rates in the (100) and (111) directions respectively. If grooves are misoriented, then ledges will form and etching of these ledges can contribute significantly to undercutting.

a) Undercutting has begun to free the Si_3N_4 mask, although the vee-grooves have not achieved their full depth.

b) In another portion of the hologram, the Si_3N_4 mask has completely lifted off and some of the peaks have begun to erode. Misorientation ledges are clearly visible on the groove sides.

Figure 4-16. Blazed, Crystalline Holographic Lens CGH104 After Etching for 12 Minutes in KOH Solution

For grooves etched in (110) silicon, Kendall [4-14] finds the etch rate of nominal (111) faces to be $r_{(111)} + 1.6\, r_{(110)}\, \Delta\Theta$ where $\Delta\Theta$ is the angular misalignment and $r_{(110)} > 400\, r_{(111)}$. Applying Kendall's results to our geometry yields a rate of undercutting $r_u = \sqrt{(3/2)}\, r_{(111)} + 1.6\, r_{(110)} \Delta\Theta$. The vee-grooves should reach their full depth before undercutting is complete if $r_{(100)} > 3\sqrt{2}\, r_u$. Adopting $r_{(100)} = r_{(110)} = 400\, r_{(111)}$ we find that complete undercutting should not occur unless $\Delta\Theta < 35$ degrees. Our holographic lenses have some misorientation of grooves with respect to the true (111) planes because of groove curvature, but this misorientation is only $\pm$ 1.1 degree for the f/16 lenses and $\pm$ 2.2 degrees for the f/8 lenses. We therefore conclude that the undercutting observed cannot be entirely attributed to misorientation.

SUMMARY

We have demonstrated all-glass computer generated holograms fabricated by e-beam lilthography and ion milling. These holograms have square-wave groove profiles, resulting in moderately high diffraction efficiencies of 40 percent. They are very environmentally durable and have a high damage threshold. They can be designed to produce wavefronts of arbitrary complexity, limited only by e-beam resolution and hologram size.

Attempts to increase diffraction efficiency to 80 percent by reducing the grating period to near 1 micron were unsuccessful because of difficulties in controlling the narrow linewidths in thick resist layers. In any event, the applicability of such ultrahigh spatial frequency holograms is marginal because of design constraints imposed by their high angular selectivity.

We also attempted to fabricate high-efficiency, blazed holograms using anisotropic etching of silicon. Undercutting of the e-beam delineated etch mask prevented us from achieving the desired groove profile. Reasons for this occurance are not fully understood. Blazed, crystalline holograms also suffer severe design constraints because of their fixed blaze angle and groove orientation.

General purpose, high-efficiency computer generated holograms will probably require a sawtooth grating profile. Others have had some success in producing such profiles in PMMA, both by e-beam lithography [4-4] and by ion milling [4-15]. We feel there is still much potential for fabricating similar structures in such durable materials as glass or quartz. At present, however, the need is for space-bandwidth product rather than high diffraction efficiency.

REFERENCES

4-1 R. Magnusson and T.K. Gaylord, "Diffraction Regimes of Transmission Gratings," J. Opt. Soc. Am. *68*, 809-814 (1978).

4-2 R.C. Enger and S.K. Case, "High-Frequency Holographic Transmission Gratings in Photoresist," to be published.

4-3 H. Nishihara, Y. Handa, T. Suhara and J. Koyama, "Direct Writing of Optical Gratings Using a Scanning Electron Microscope," Appl. Opt. *17*, 2342-2345 (1978).

4-4 T. Fujita, H. Nishihara and J. Kayama, "Blazed Gratings and Fresnel Lenses Fabricated by Electron-Beam Lithography," Opt. Lett. *7*, 578-580 (1982).

4-5 M.G. Moharam and T.K. Gaylord, "Diffraction Analysis of Dielectric Surface-Relief Gratings," J. Opt. Soc. Am. *72*, 1385-1392, (1982); erratum *73*, 411 (1983).

4-6 F.G. Kaspar, "Diffraction by Thick, Periodically Stratified Gratings with Complex Dielectric Constant," J. Opt. Soc. Am. *63*, 37-45 (1973).

4-7 C.B. Burckhardt, "Diffraction of a Plane Wave at a Sinusoidally Stratified Dielectric Grating," J. Opt. Soc. Am. *56*, 1502-1509 (1966).

4-8 L.D. Westbrook, A.W. Nelson and C. Dix, "High Quality InP Surface Corrugations for 1.55μm InGaAsP DFB Lasers Fabricated Using Electron-Beam Lithography," Electron. Lett. *20*, 863-865, (1982).

4-9 K.E. Bean, "Anisotropic Etching of Silicon," IEEE Trans. on Electron Devices *ED-25*, 1185-1193 (1978).

4-10 E. Bassous, "Fabrication of Novel Three-Dimensional Microstructures by the Anisotropic Etching of (100) and (110) Silicon," IEEE Trans. on Electron Devices *ED-25*, 1178-1185 (1978).

4-11 K.E. Petersen, "Dynamic Micromechanisms on Silicon: Techniques and Devices," IEEE Trans. on Electron Devices *ED-25*, 1241-1250 (1978).

4-12 D.B. Lee, "Anisotropic Etching of Silicon," J. Appl. Phys. *40*, 4569-4574 (1969).

4-13 E.G. Loewen, M. Nevière and D. Maystre, "Grating Efficiency Theory as it Applies to Blazed and Holographic Gratings," Appl. Opt. *16*, 2711-2721 (1977).

4-14 D.L. Kendall, "On Etching Very Narrow Grooves in Silicon," Appl. Phys. Lett. *26*, 195-198 (1975).

4-15 Y. Aoyagi and S. Namba, "Blazed Ion-Etched Holographic Gratings," Optica Acta *23*, 701-707 (1976).

Section 5
Summary of Accomplishments

HOLOGRAM WRITING CAPABILITY

- Achieved e-beam writing with a line-centering accuracy of ±0.2 microns, or 0.004 percent over a 1-cm diameter image.
- Identified optical plotter distortion (DICOMED Image Recorder) to be 0.05 percent, with usable resolution of 2000 pixels per diameter.
- Developed versatile and efficient encoding algorithms permitting routine fabrication of e-beam computer generated holograms.

APPLICATIONS OF E-BEAM COMPUTER GENERATED HOLOGRAMS

- Demonstrated use of e-beam computer generated holograms in testing of 4-inch f/2 parabola and asymmetric deep aspheric surfaces.
- Supplied about 50 e-beam computer generated holograms to Honeywell Electro-Optics Division for aspheric testing of diamond-turned surfaces.
- Proposed and developed an optical vector-matrix multiplication scheme utilizing spatially partitioned, computer generated holograms (PCGHs) to achieve high numerical accuracy and large numerical range.
- Demonstrated PCGHs with 20-dB numerical accuracy and 37-dB numerical range in 1 × 10 matrix operations.

HIGH DIFFRACTION EFFICIENCY, COMPUTER GENERATED HOLOGRAMS

- Developed fabrication techniques for producing 40-percent efficient, environmentally durable, all-glass holograms with grating periods as small as 2.5 microns.
- Investigated anisotropic etching techniques for producing blazed, reflection holograms in silicon.

The reverse of this page is blank.

Appendix
Miscellaneous Information

PERSONS WHO PARTICIPATED IN THE RESEARCH

S.M. Arnold, Principal Investigator

K.M. Leung, Principal Investigator (Jan 1980 to May 1981)

F.M. Schmit, Senior Research Scientist

J.C. Lindquist, Research Scientist

H.M. Zimmermann, Research Scientist, Honeywell Solid State Electronics Division

S.K. Case, Consultant, Assistant Professor of Electrical Engineering at the University of Minnesota

J.C. Wyant, Consultant, Professor of Optical Sciences at the University of Arizona

PUBLICATIONS

K.M. Leung, J.C. Lindquist and L.T. Shepherd, "E-beam Computer Generated Holograms for Aspheric Testing," Proc. Soc. Photo-Opt. Instrum. Eng. 215, 70-75, (1980).

S.M. Arnold and S.K. Case, "E-beam Generated Holographic Masks for Optical Vector-Matrix Multiplication," presented at NASA conference on Optical Information Processing for Aerospace Applications, NASA Conf. Pub. 2207, 309-317 (1981).

S.M. Arnold and S.K. Case, "E-beam Generated Holographic Masks for Optical Vector-Matrix Multiplication," accepted for publication in Opt. Eng.

OTHER ACTIVITIES

Transferred technology of aspheric testing using computer generated holograms to Honeywell Electro-Optics Division in March of 1980.

Distribution

AFOSR CONTRACTORS AND GRANTEES

Dr. Joe T. Boyd
Department of Electrical Engineering
University of Cincinnati
Cincinnati, Ohio 45221

Dr. David Casasent
Carnegie-Mellon University
Department of Electrical Engineering
Pittsburgh, Pennsylvania 15213

Dr. William S.C. Chang
Department of Electrical Engineering
& Computer Science
University of California, San Diego
La Jolla, California 92093

Dr. Steven K. Case
Department of Electrical Engineering
University of Minnesota
Minneapolis, Minnesota 55455

Dr. George Eichmann
Department of Electrical Engineering
The City University of New York
Covent Avenue at 138th Street
New York, New York 10031

Dr. Nabil H. Farhat
Moore School of Electrical Engineering
University of Pennsylvania
Philadelphia, Pennsylvania 19174

Dr. Nicholas George
Director, Institute of Optics
The University of Rochester
Rochester, New York 14627

Dr. Joseph W. Goodman
Department of Electrical Engineering
Stanford Electronics Laboratories
Stanford University
Stanford, California 94305

Dr. Bobby R. Hunt
Systems & Industrial Engineering Department
University of Arizona
Tucson, Arizona 85721

Mr. Peter Kellman
ESL Incorporated
495 Java Drive
Sunnyvale, California 94086

Dr. Sing H. Lee
Department of Applied Physics and
Information Science
University of California, San Diego
La Jolla, California 92093

Mr. Kenneth Leib
Research Department
Grumman Aerospace Corporation
South Oyster Bay Road
Bethpage, New York 11714

Professor Emmett N. Leith
Electrical and Computer Engineering Department
The University of Michigan
Ann Arbor, Michigan 48109

Dr. William T. Rhodes
School of Electrical Engineering
Georgia Institute of Technology
Atlanta, Georgia 30332

Dr. Alexander A. Sawchuk
Electrical Engineering Department
University of Southern California
Los Angeles, California 90007

Mr. Bernard Soffer
Opto-Electronics Department
Hughes Research Laboratories
3011 Malibu Canyon Road
Malibu, California 90265

Dr. C.S. Tsai
Department of Electrical Engineering
The University of California - Irvine
Irvine, California 92717

Dr. Carl M. Verber
Battelle-Columbus Laboratories
505 King Avenue
Columbus, Ohio 43201

Dr. John Walkup
Department of Electrical Engineering
Texas Tech University
Lubbock, Texas 79409

Dr. Cardinal Warde
Electrical Engineering & Computer Science
Massachusetts Institute of Technology
Cambridge, Massachusetts 02139

Dr. Richard Williamson
Lincoln Laboratory
Massachusetts Institute of Technology
Lexington, Massachusetts 02173

Dr. Francis T.S. Yu
Department of Electrical Engineering
Pennsylvania State University
University Park, Pennsylvania 16802

Supplemental Distribution List

Dr. Gerald Brandt
Westinghouse Research & Development Center
1310 Beulah Road
Pittsburgh, Pennsylvania 15235

Dr. Keith Bromley
Code 8111
Naval Ocean Systems Center
San Diego, California 92152

Dr. Robert Brooks
TRW Systems Group
R1/1062 One Space Park
Redondo Beach, California 90278

Dr. F. Paul Carlson
Applied Physics and Electronic Science
Oregon Graduate Center
19600 N.W. Walker Road
Beaverton, Oregon 97005

Professor W. Thomas Cathey
Department of Electrical Engineering
University of Colorado
Denver, Colorado 80302

Dr. H.J. Caulfield
Aerodyne Research, Inc.
Applied Science Division
Bedford Research Park
Bedford, Massachusetts 01730

Dr. B. Jin Chang
Kaiser Optical Systems
P.O. Box 983
Ann Arbor, Michigan 48106

Mr. Ivan Cindrich
Environmental Research Institute of Michigan
P.O. Box 8618
Ann Arbor, Michigan 48107

Professor Stuart A. Collins, Jr.
Department of Electrical Engineering
Ohio State University
2015 Neil Avenue
Columbus, Ohio 43210

Dr. Jim Constantine
AD/AFATL/DLJ
Eglin AFB, Florida 32542

Chief, Electro Optics Technology Branch
AFAL/DHO
Wright-Patterson AFB, Ohio 45433

Dr. Albert Friesem
Weizmann Institute of Science
Rehovot, Israel

Dr. Bobby Guenther
Army Research Office
P.O. Box 12211
Research Tringle Park, North Carolina 27709

Dr. Richard Hudgins
Itek Corporation
10 Maguire Road
Lexington, Massachusetts 02173

Dr. John N. Lee
Code 6530
Naval Research Laboratory
Washington, DC 20375

Dr. Robert D. Leighty
Research Institute
U.S. Army Engineer Topographic Laboratories
Fort Belvoir, Virginia 22060

Professor Adolf Lohmann
Physics Institute
University of Erlangen-Nurnberg
Erwin-Rommel-Strasse
D 8510 Erlangen
F.R. Germany

Mr. Bob V. Markevitch
Ampex Corporation
401 Broadway
Redwood City, California 94063

Dr. Robert Marks
Department of Electrical Engineering
University of Washington
Seattle, Washington 98195

Dr. Richard Mergerian
Westinghouse Electric Corporation
P.O. Box 1521
Mail Stop 3714
Baltimore, Maryland 21203

Mr. Bill Miceli
RADC/ESOP
L.G. Hanscom AFB, Massachusetts 01731

Dr. Robert A. Sprague
Xerox Corporation
Palo Alto Research Labs
3333 Coyote Hill Road
Palo Alto, California 94304

Mr. Eric Stevens
Code 7924S
Naval Research Laboratory
Washington, D.C. 20375

Dr. William Stoner
Systems Applications, Inc.
3 Preston Court
Bedford, Massachusetts 01730

Dr. Henry Taylor
Code 6570
Naval Research Laboratory
Washington, D.C. 20375

Professor Brian Thompson, Dean
School of Engineering
University of Rochester
Rochester, New York 14627

Mr. Terry Turpin
NSA R551
9800 Savage Road
Fort Meade, Maryland 20755

Dr. Anthony Vander Lugt
232 Cocoa Avenue
Indialantic, Florida 32903

Dr. Bernard Vatz, Radar Directorate
BMDATC
P.O. Box 1500
Huntsville, Alabama 35807

Dr. Harper Whitehouse
Code 6003
Naval Ocean Systems Center
San Diego, California 92152

Professor James Wyant
Optical Sciences Center
University of Arizona
Tucson, Arizona 85721

The reverse of this page is blank.

END

FILMED

10-83

DTIC